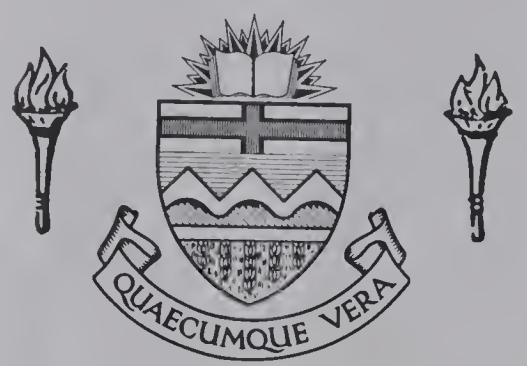

The University of Alberta
Printing Department
Edmonton, Alberta

THE UNIVERSITY OF ALBERTA

THE $^{20}Ne(d,n)^{21}Na$ REACTION, THE STATES OF ^{21}Na AND FOUR THEORIES

by

Geoffrey George Frank

A THESIS

SUBMITTED TO THE FACULTY OF GRADUATE STUDIES

IN PARTIAL FULFILLMENT OF THE REQUIREMENTS FOR THE DEGREE

OF MASTER OF SCIENCE

DEPARTMENT OF PHYSICS

EDMONTON, ALBERTA

July, 1968

UNIVERSITY OF ALBERTA

FACULTY OF GRADUATE STUDIES

The undersigned certify that they have read, and recommend to the Faculty of Graduate Studies for acceptance, a thesis entitled THE $^{20}Ne(d,n)^{21}Na$ REACTION, THE STATES OF ^{21}Na AND FOUR THEORIES, submitted by Geoffrey George Frank in partial fulfillment of the requirements for the degree of Master of Science.

ACKNOWLEDGEMENTS

I would like to thank the following people:

(1) my supervisor, Dr. W.J. McDonald, for his support and many helpful suggestions during the course of this research, especially his help in setting up the neutron time-of-flight electronics;

(2) Mr. M.B. Burbank, for his work on the detector efficiency, his original design of the gas target system and his help in the early stages of the neon work;

(3) Mr. N.E. Davison, for his help with both the Hauser-Feshbach and Nilsson Model computer programs;

(4) Mr. T.H. Hsu, for his help in getting a useful beam during the experiments;

(5) Mr. J.B. Elliott and his staff, for the maintenance of the machine and Mr. L. Holm for the maintenance of the SDS-920 computer;

(6) Dr. S.S.M. Wong, who did the Shell Model calculations;

(7) Miss E. Hawirko for the typing of the manuscript.

Finally I would like to thank the University of Alberta for providing financial support for the duration of this research.

TABLE OF CONTENTS

LIST OF FIGURES

LIST OF TABLES

ABSTRACT

Absolute differential cross-sections are obtained for neutron groups corresponding to the four bound states of ^{21}Na reached via the $^{20}Ne(d,n)^{21}Na$ reaction at E_d = 5.16 and 6.08 MeV. These cross-sections are compared to a sum of direct interaction and compound nucleus model predictions based on DWBA and Hauser-Feshbach theories. Absolute spectroscopic factors are extracted and are compared with the predictions of the Nilsson and Shell Model descriptions for ^{21}Na.

CHAPTER I

INTRODUCTION

1.1 Motivation

The reason for doing a nuclear reaction of the type A(a,b)B is to learn more about:

(a) the make-up of the residual nucleus B

(b) the forces of interaction between A and a and between B and b

(c) the possible formation of a compound nucleus -

$$A + a \rightarrow A^* \rightarrow B + b$$

In general, the procedure in a physics experiment is to postulate some kind of theory, then test the theory by comparing its predictions to the results of the experiment. In the present study of the $^{20}Ne(d,n)^{21}Na$ reaction, absolute cross-sections are measured for neutron groups corresponding to the bound states of ^{21}Na at deuteron bombarding energies of 3.92, 5.16 and 6.08 MeV, and it is our aim to provide a test of the Nilsson Model, the Shell Model, Distorted Wave Born Approximation (DWBA) theory and Hauser-Feshbach (HF) theory for this special case. The first two fall under point (a) above, while the DWBA and HF theories fall under (b) and (c). The experimental angular distributions are compared to a sum of theoretical compound nucleus (Hauser-Feshbach) and direct interaction (DWBA) parts, and absolute spectroscopic factors are extracted for the bound states of ^{21}Na. These spectroscopic factors along with the

excitation energies of the low-lying levels of ^{21}Na are compared to the predictions of two models of the nucleus: the Nilsson and Shell Models.

The ^{20}Ne(d,n)^{21}Na reaction was chosen for a number of reasons. The best comparison between theory and experiment occurs when the cross-sections are in absolute terms, and to get the most accurate absolute cross-sections, a gaseous target should be used as the thickness of a gas target is known more accurately. Sophisticated DWBA programs are available for single nucleon transfer stripping reactions and the University of Alberta laboratory has a good facility for the detection of neutrons by the time-of-flight method; hence the (d,n) reaction was chosen. The Nilsson and Shell Models have had good success for nuclei in the s-d shell (Bh 62, Go 60, Ku 67, Ha 67, Wo 68); in particular, there is apparent success for the Nilsson Model for nuclei of mass 21 and 23 (Ho 65) although the experimental evidence is rather weak for ^{21}Na and ^{23}Mg. A shell model program is available which when used with the effective interaction of Kuo (Ku 67) has been successful in predicting the properties of many s-d shell nuclei. Hence, the choice of reaction was ^{20}Ne(d,n)^{21}Na.

There is the possibility of an undiscovered low-lying level in ^{21}Na. A doublet could be possible at an excitation of 2.41 MeV, corresponding to the doublet at 2.80 MeV observed in the mirror nucleus, ^{21}Ne (Pr 67). Thus, a secondary reason for looking at ^{21}Na is the search for this possible level.

It was decided to run the experiment at three widely spread deuteron energies to achieve a better comparison between experimental results and

theoretical predictions. The 3.92 MeV experimental work was done by M.B. Burbank (Bu 67).

1.2 Previous Studies of ^{21}Na

Experimentally, the ^{20}Ne(d,n)^{21}Na reaction has been studied by a number of groups. Benenson and Lidofsky (Be 61), using E_d = 4.87 MeV and a gas recoil spectrometer, extracted absolute cross-sections and reduced widths for the bound states of ^{21}Na but were hindered by limitations in energy resolution and detector efficiency calibration. Ajzenberg-Selove et al (Aj 61) employed the time-of-flight technique and energies of 2.4, 3.1, 4.6 and 6.1 MeV to get absolute cross-sections and reduced widths, but they too had resolution difficulties. Grüebler and Rossel (Gr 61) obtained absolute cross-sections and reduced widths for the ground and first excited states at E_d = 2.83 MeV as did Pessoa (Pe 65) at E_d = 1.3 to 2.3 MeV. ^{21}Na was also studied via the (d,nγ) reaction at E_d less than 3.0 MeV by Gibbs and Grüebler (Gi 65) and via the (p,γ) reaction by van der Leun and Mouton (Va 64).

The present study should be a significant improvement over the previous (d,n) studies as the resolution of the neutron spectrometer is much better and the highly-developed DWBA theory is used instead of the Plane Wave Born Approximation (PWBA) to extract spectroscopic factors. The estimation of the compound nucleus contribution to the cross-sections corresponding to the various states should also improve the results.

CHAPTER II

THE EXPERIMENT

2.1 Beam Transport System

The time-of-flight technique is the best method available at present for the energy measurement of neutrons. Both high resolution and large range of neutron energies are significant features of this technique. Since the neutron flight times encountered are in the nanosecond region, very short ion bursts of high intensity are required. The University of Alberta beam transport system, consisting of a 6 MeV Van de Graaff accelerator† and Mobley compression system, employs both pre-acceleration pulsing and post-acceleration compression to satisfy this requirement (see fig. 2-1).

Deuterium gas is ionized within a source bottle at the high voltage terminal by a 125 MHz. source oscillator and is emitted by means of a probe electric field. The beam starts to accelerate towards zero voltage down the tube. It is focussed by the Einzel lens and Terminal Analysis Magnet at a 1/16 inch aperture and can be pulsed by sweeping it in an elliptical pattern over this aperture by two pairs of RF deflection plates, set at right angles to each other. An RF frequency of 1 MHz. produces a beam pulse of 10 ns. width which is focussed by 'Focus 3' and the self-focussing column before reaching the momentum Analyzing

---

† High Voltage Engineering Corp., Burlington, Mass., U.S.A.

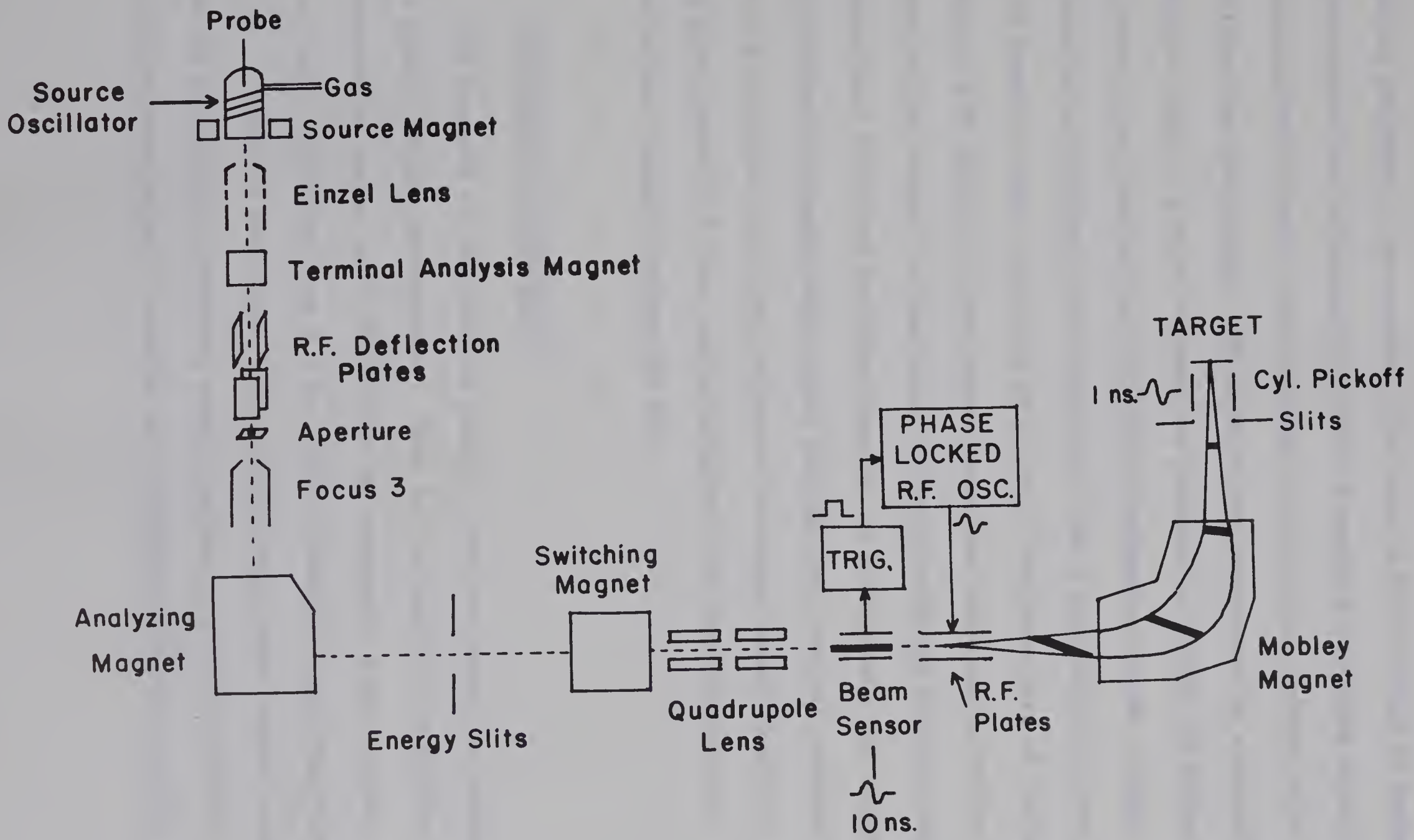

Fig. 2–1 : Beam Transport System

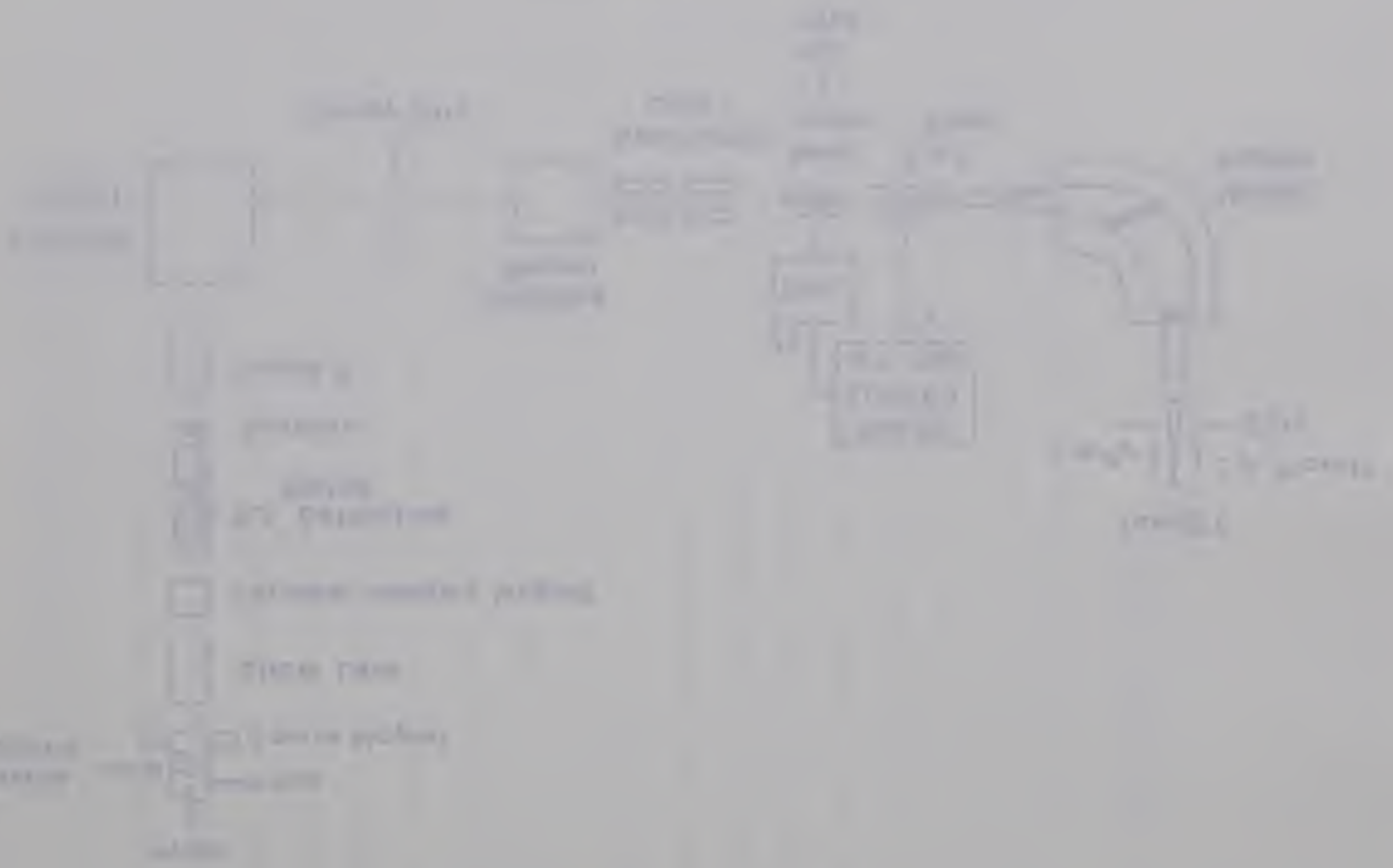

Magnet at the base of the machine. The beam is bent through 90 degrees by this magnet and refocussed at a pair of energy stabilizing slits 57 inches away which feed a control system for the corona current which stabilizes the beam energy. The beam is then refocussed by a magnetic quadrupole lens to a point between the plates of a 10 MHz. RF deflection oscillator, the first part of the Mobley compression system. Phase information is supplied to the oscillator from a cylindrical pick-off in the beam tube just before the RF plates. The other part of the Mobley system is a 90 degree, 75 inch magnet which has focal points at the RF plates and the target. A beam burst is swept by the RF field in such a manner that the first particles leaving the plates take the longest paths through the magnet while those leaving last take the shortest so that all particles in a burst arrive at the target simultaneously. A beam pulse width of 0.4 ns. can be obtained with the University of Alberta beam transport system (Mc 67).

2.2 The Neutron Spectrometer

The energies of the neutrons emitted from the target are measured by a time-of-flight spectrometer. That is, the particle velocities are determined by timing their flight over an accurately known distance. The stop signal originates from a 3 cm. long cylindrical capacitor which is 30 cm. in front of the target. The corresponding start signal originates from the main neutron detector, which consists of a Philips XP1040 photo-multiplier tube optically coupled to a cylindrical (3.45" x 0.75") quartz

container filled with Ne 213[†] liquid scintillator. This detector sits on a remote-controlled cart which can be moved through angles from 0 to 150 degrees and distances from the target of 1.0 to 6.3 metres. There is also a monitor detector held in a fixed position for the normalization of angular distributions. It consists of a Naton phosphor[*] coupled to an RCA 8575 photomultiplier tube. The monitor system uses the same stop pulse as the main system.

The reason for using the capacitive pick-off for the stop signal instead of for the start signal is that the dead time of the system is decreased. If no neutron is detected for a given ion burst, the system still remains ready for the next burst.

The electronics diagram for the spectrometer is shown in fig. 2-2. The photomultiplier anode signal is fed to a Constant Fraction Pulse Height Trigger (CFPHT). By triggering at a constant fraction of the pulse height on the leading edge of the pulse, changes in the timing of the start trigger point with respect to the stop trigger point due to variations in the detector pulse size ("walk") can be eliminated. A fraction of about 1/10 is chosen for the best time resolution (Ge 67). In the stop channel, the zero-crossover point of the bipolar pickoff signal is used as the stop trigger point (Ge 67a).

The start and stop pulses are fed to an Ortec Model 437 Time-to-Amplitude Convertor (T.A.C.) (#1). This T.A.C. normally outputs a

---

† Nuclear Enterprises Ltd., Winnipeg, Manitoba.

* Nash & Thompson Ltd., Hookrise South, Tolworth, Surrey, England.

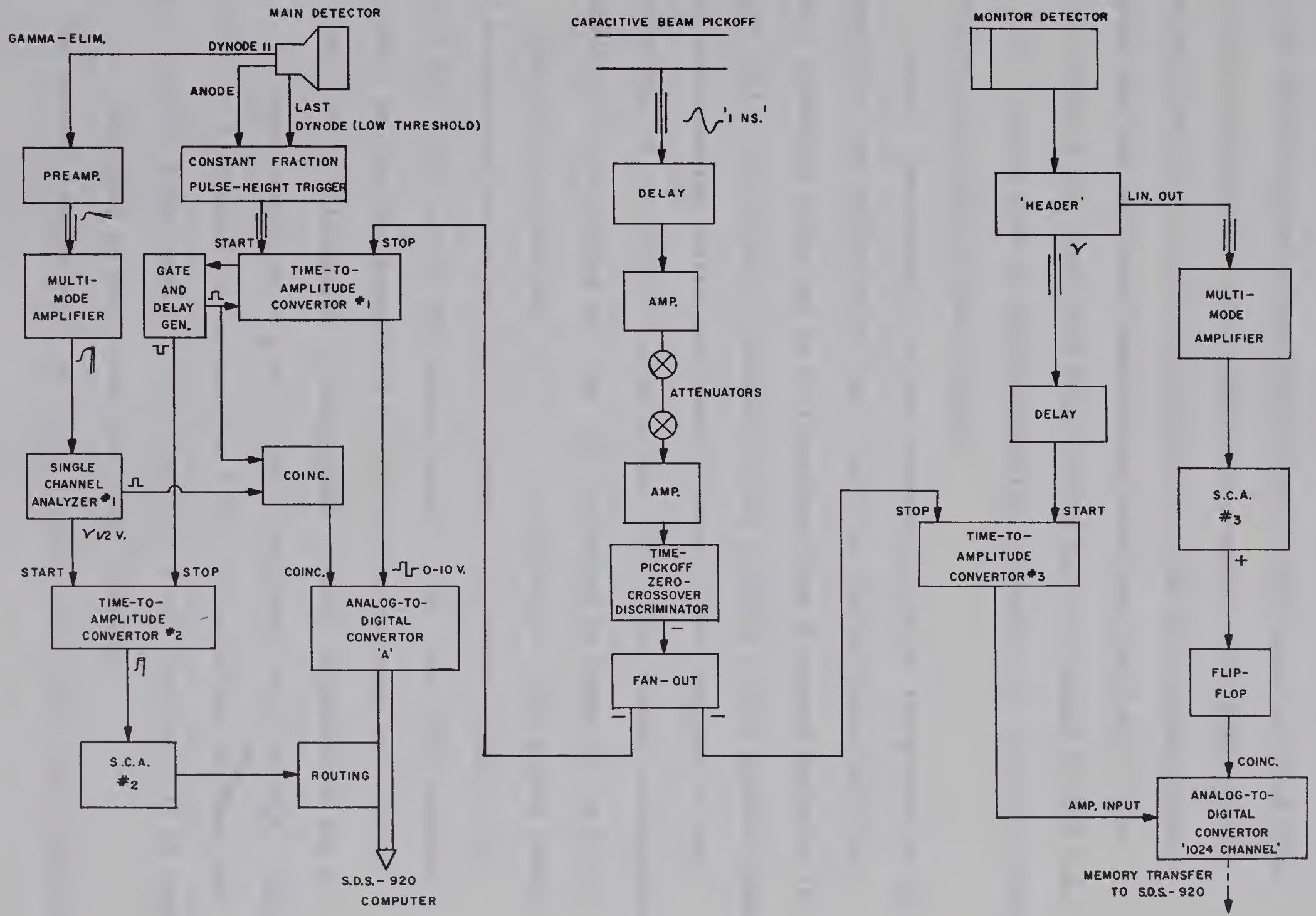

Fig. 2—2 : Time-of-Flight Electronics

pulse when the stop pulse is sensed. Since a coincidence is necessary for the identification of detector pulses in this case, we would like the T.A.C. output pulse to be timed with respect to the start pulse. To accomplish this, a pulse corresponding to the start pulse is fed through the Gate and Delay Generator and back into the T.A.C. The T.A.C. output pulse comes when this delayed pulse is sensed by the T.A.C. The T.A.C. output goes to Analog-to-Digital Convertor 'A' (A.D.C.A.) which feeds the S.D.S.-920 on-line computer.

A signal from dynode 11 of the photomultiplier is integrated by the Preamplifier and double-delay-line clipped in the Multimode Amplifier. Since a gamma-ray pulse can be distinguished from a neutron pulse by its longer tail, the process of integration and clipping yields bipolar pulses whose zero-crossing points are timed differently with respect to the leading edge of the detector anode pulse. Thus those pulses corresponding to neutrons can be picked out from all the pulses by means of the T.A.C. #2 - Single Channel Analyzer (S.C.A.) #2 combination. The pulses identified as neutrons are routed into the second 2048-channel range by the routing unit; the rest of the pulses remain in the first 2048 channels. The result is that the background in the neutron spectrum is reduced.

For further elimination of background, a lower threshold is set by S.C.A. #1 whose output pulse goes to the coincidence input of ADCA. There must also be a coincidence between the S.C.A. #1 pulse and the Gate and Delay Generator pulse when the SCA threshold is set (section 2.3) in case the S.C.A. threshold is lower than the CFPHT threshold.

The monitor circuit need not be as sophisticated since time resolution

is not of prime importance here and we need not eliminate the pulses corresponding to gamma-rays. A lower threshold can be set by S.C.A. #3 to decrease background. The monitor spectrum is stored in the '1024-channel' A.D.C. and can be dumped into the computer memory on command.

All data is easily transferred to magnetic tapes for storage purposes.

2.3 Detector Efficiency

Since absolute cross-sections are to be measured, the absolute efficiency of the neutron detector is of major importance. The relative efficiency curve was measured by doing angular distributions of the $T(p,n)^3He$ and $D(d,n)^3He$ reactions at E_p = 3.00 MeV and E_d = 3.52 MeV and normalizing the data to that published by Goldburg (Go 61) and Brolley and Fowler (Br 60). This covered a neutron energy range up to 6.8 MeV. The relative curve was then normalized to two points of an absolute determination (Bu 67) which utilized the associated particle $D(d,n)^3He$ reaction. Both neutrons and ^3He particles are detected in this method, the latter with 100% efficiency. The error in the relative curve is 5% while that of the absolute curve is estimated by Burbank to be 7%.

The shape and magnitude of the efficiency curve is highly dependent upon the lower threshold as determined by S.C.A. #1 and so a method must be found whereby the same threshold is obtained for each experiment. The method used at Alberta is the following: a ^{22}Na gamma-ray source is set up in front of the scintillator and, employing the electronics setup of

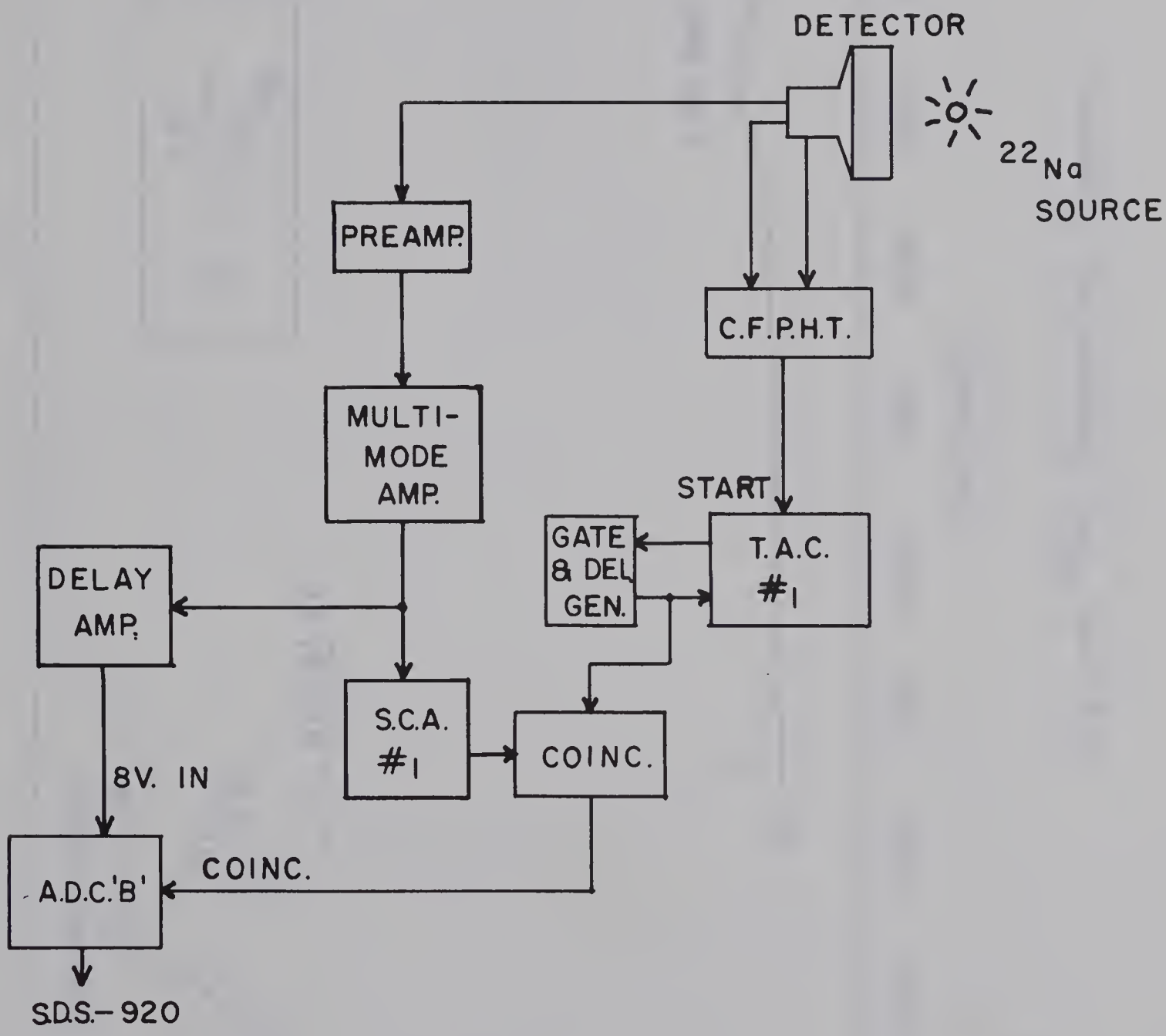

Fig. 2—3 :'CUTOFF' ELECTRONICS

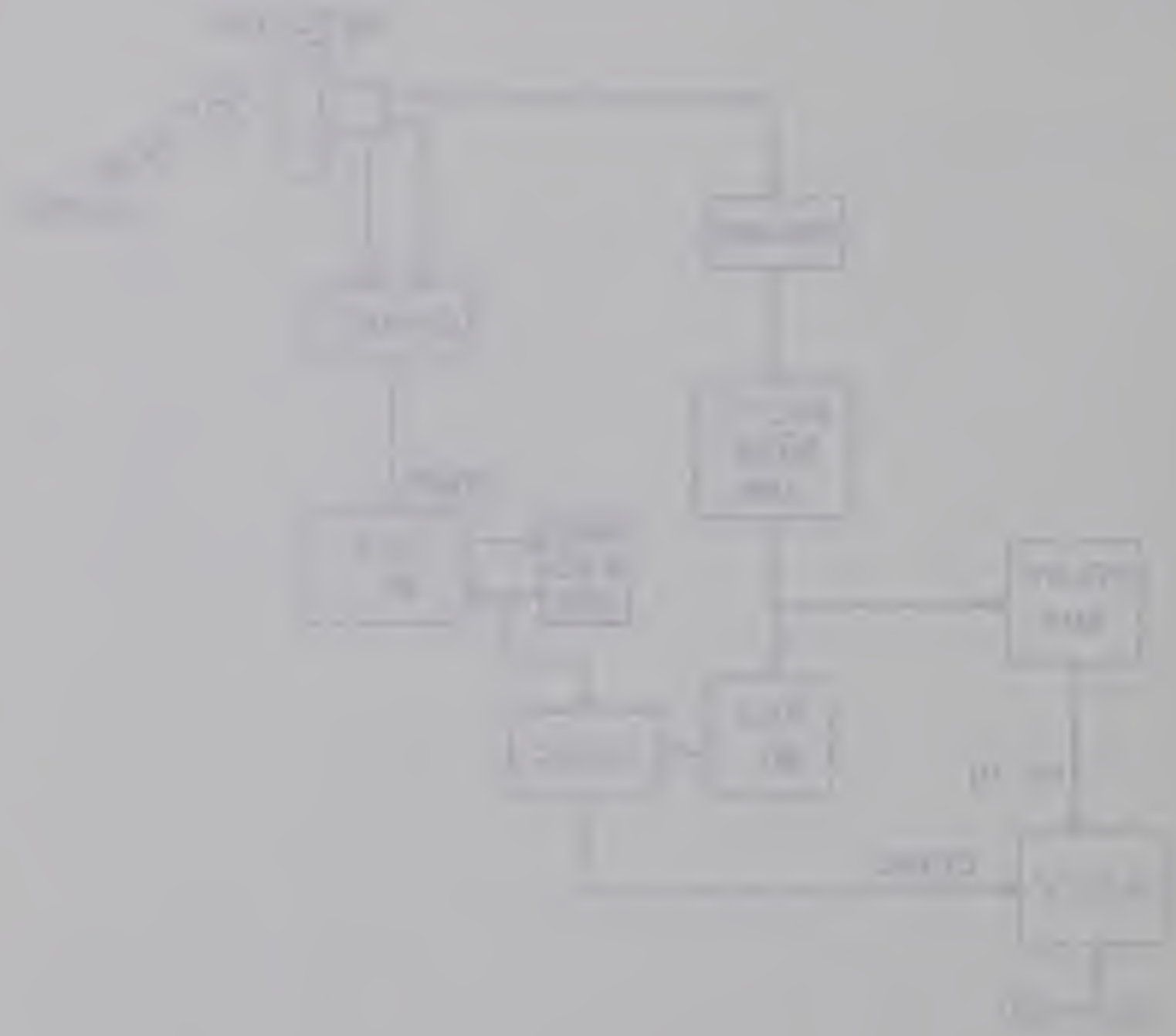

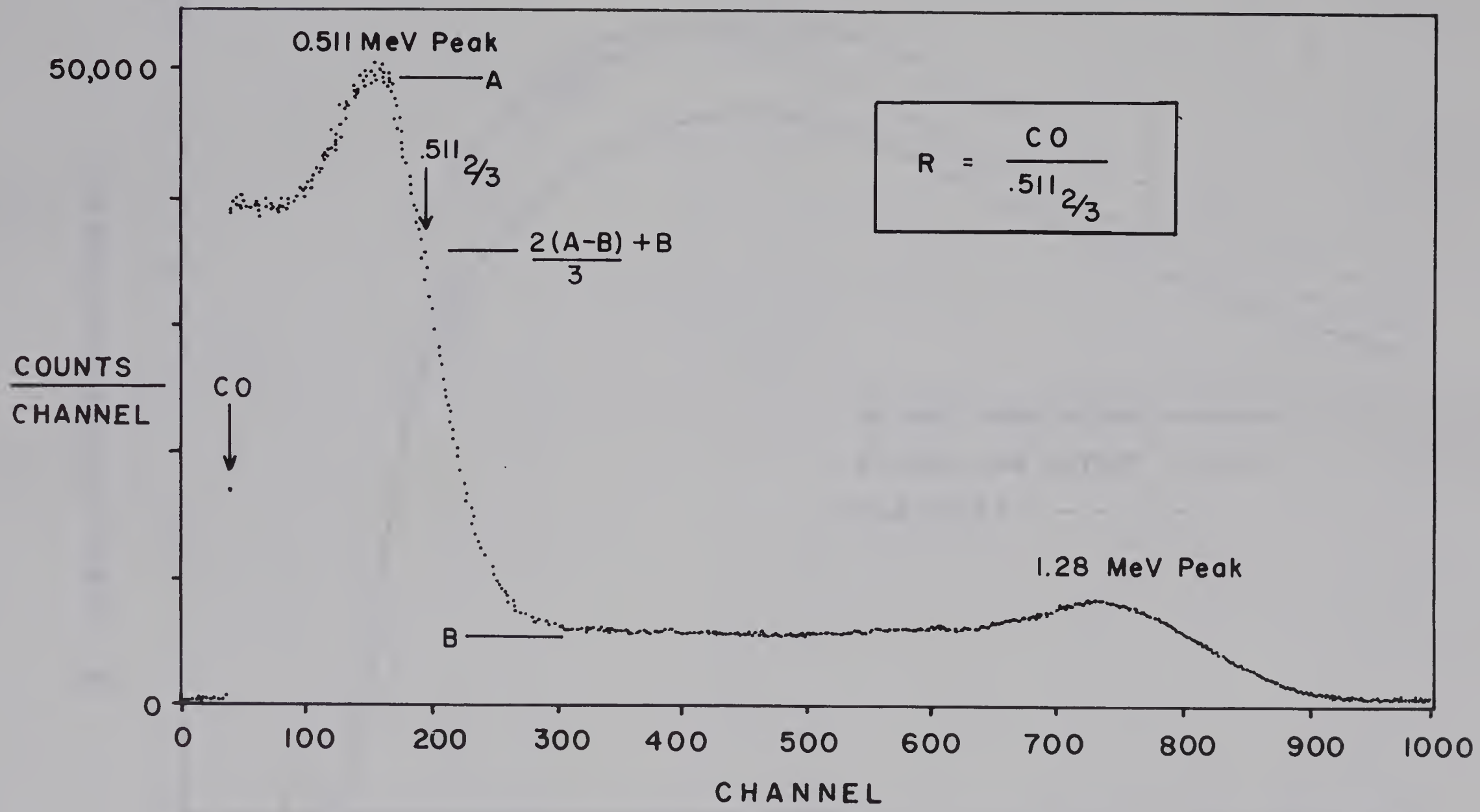

Fig. 2-4: ^{22}Na Gamma-Ray Spectrum

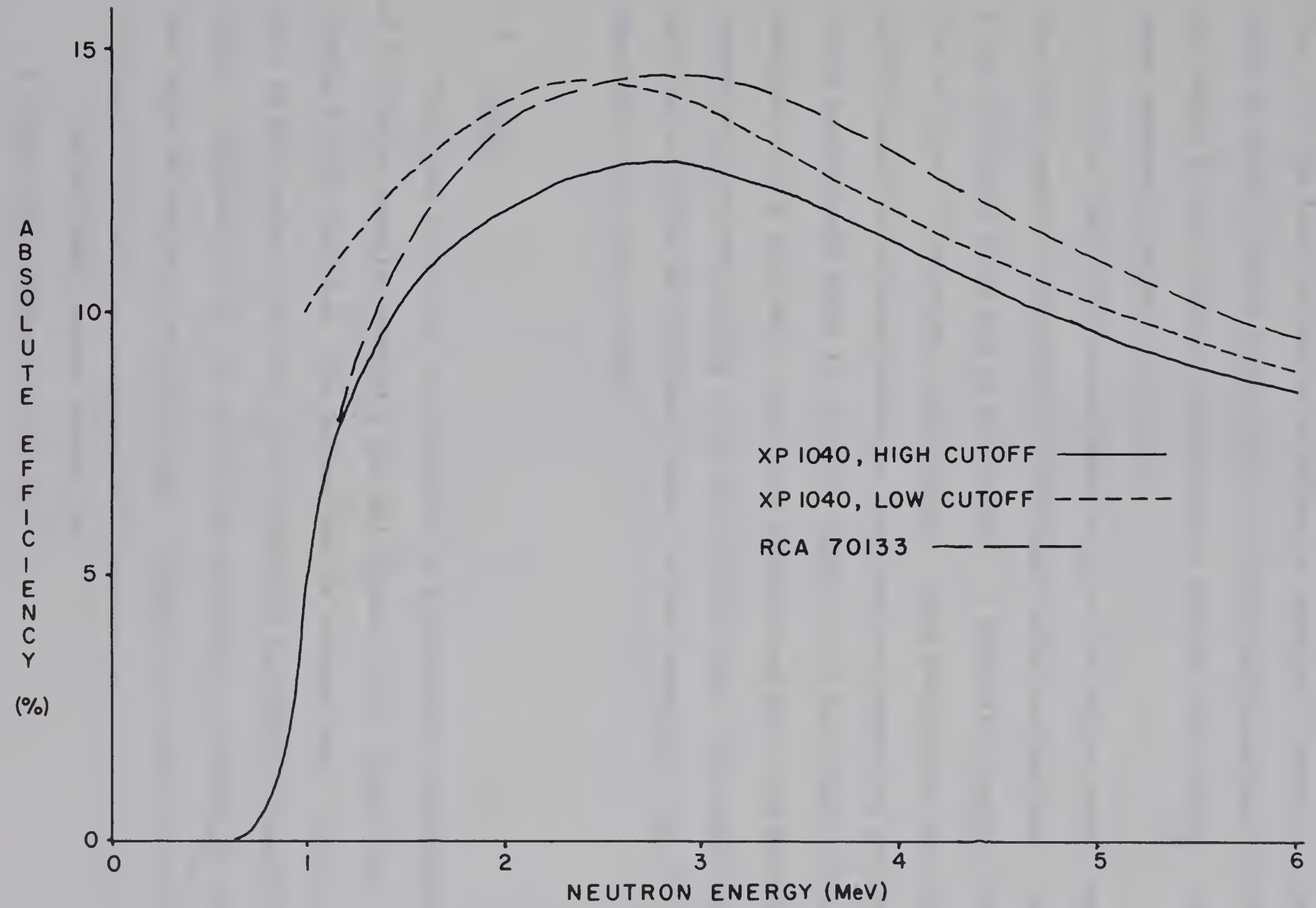

Fig. 2-5: Absolute Efficiency Curves

fig. 2-3, the lower threshold is defined in terms of R where R is the ratio of cutoff neutron energy (C.O.) to energy corresponding to 2/3 of the height of the 0.511 MeV characteristic peak of ^{22}Na ($0.511_{\frac{2}{3}}$). The gamma spectrum is shown in fig. 2-4.

For the ^{20}Ne(d,n)^{21}Na experiment at E_d = 5.16 MeV, a cutoff lower than that used for the determined efficiency curve was employed. Thus a new efficiency curve had to be obtained. A ^{9}Be(α,n)^{12}C angular distribution at E_d = 4.5 MeV served this purpose. Using the routing unit, both cutoffs could be run simultaneously. All that are needed are the ratios of the neutron peak areas for the two cutoffs. For the ^{20}Ne(d,n)^{21}Na reaction at E_d = 6.08 MeV, a different detector was used - an RCA C70133 photomultiplier tube coupled to an Ne218 scintillator. The same technique was used to obtain the efficiency curve for this detector. Fig. 2-5 shows all 3 efficiency curves.

2.4 Target

The target cell, fig. 2-6, consists of a rectangular parallelepiped of 0.010-inch tantalum epoxied†, top and bottom, to two copper discs forming a leak tight box. The bottom disc is screwed into a copper base which is air cooled. The cell can be evacuated and filled through the bottom. Platinum foil of 100 micro-inch thickness is epoxied* to 3/8-inch holes in the cell, front and rear. Platinum was chosen as it gives

---

† Plastic Steel, Devcon Canada Ltd.

* Epoxy Glue, Borden Chemical Co.

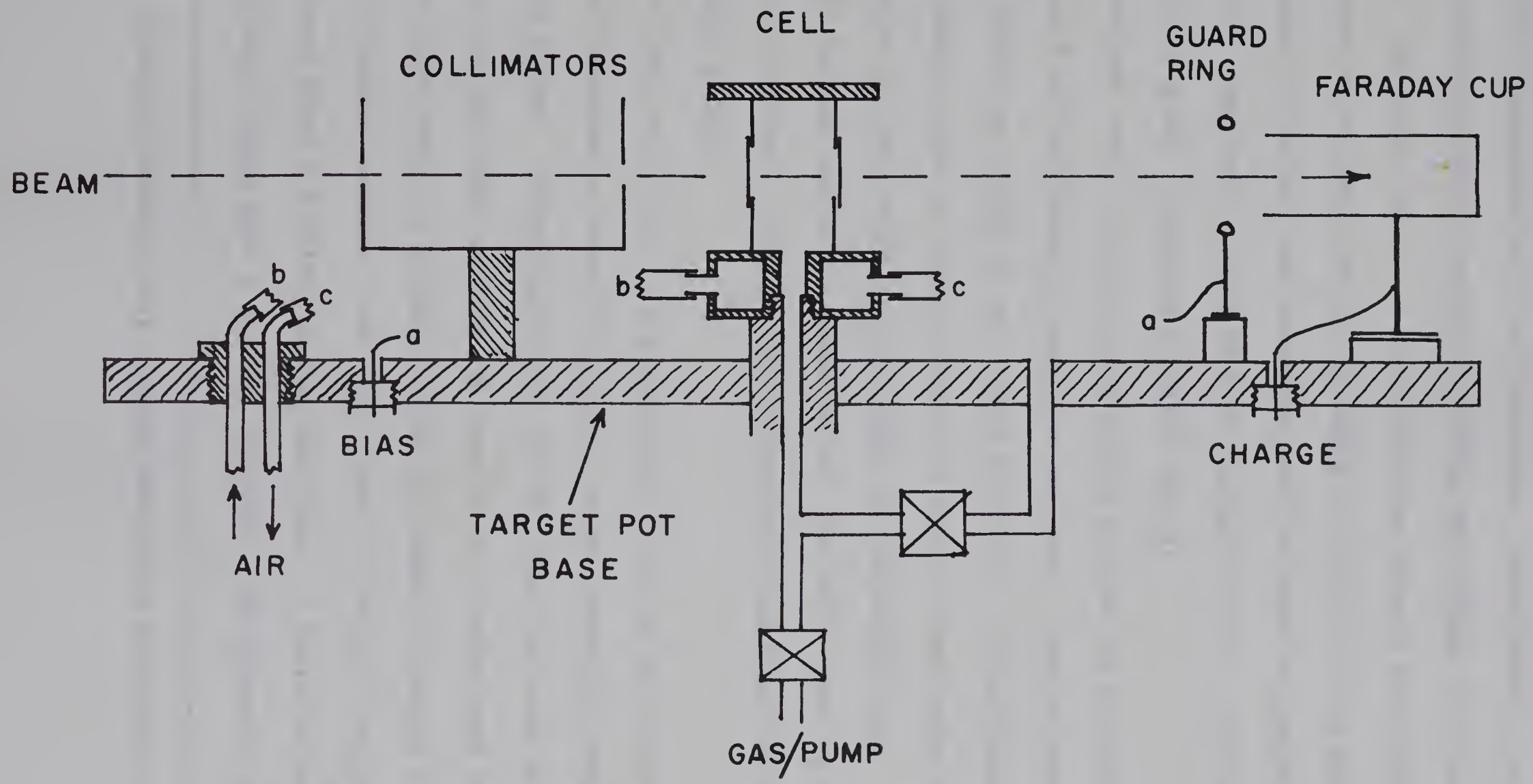

Fig. 2-6: Gas Target Setup

negligible background for 6 MeV deuterons. Unfortunately, no thinner than 100 micro-inch Pt. could be used as the thinner foils are not leak tight. The energy loss of a 6 MeV deuteron through the front foil was determined to be about 200 keV by doing a $^{9}Be(d,n)^{10}B$ run with a solid ^{9}Be target in the cell and repeating with the same ^{9}Be target without the cell. The result agrees with the energy loss for a 100 micro-inch Pt. foil as given in Whaling's tables (Wh 58).

The beam could not be stopped in the cell as the air cooled heat sink could not sufficiently dissipate the heat. Thus the beam is collected in a Faraday cup placed 10 cm. behind the cell. Two collimators with 1/8-inch diameter holes in front of the cell serve to make sure the beam does not strike the cell walls and is caught in the Faraday cup. A guard ring near the Faraday cup with a potential of -300 volts isset up to repel secondary electrons. The charge is measured by an Elcor current integrator (Model A309A).

The cell was filled to a pressure of 20 cm. of Hg., corresponding to a target thickness of about 250 $\mu g/cm^2$, using a specially designed gas-handling system. Isotopically pure (99.9%) ^{20}Ne[†] was used as the target gas. As the gas heats up when the beam is on, a valve near the cell entrance pipe should be closed so that the number of nuclei in the beam path will remain constant. Any large leaks in the cell can be detected by a Pirani gauge a few feet up the beam tube. A valve in the beam tube automatically closes when a leak is detected. The pressure can be checked

---

[†] Monsanto Research Corp., Mound Laboratory, Miamisburg, Ohio, U.S.A.

by opening the entrance pipe valve after the beam has been shut off for a while to let the gas get back to room temperature.

CHAPTER III

DATA ANALYSIS

3.1 Excitation Energies

Using the beam transport system, neutron spectrometer and target setup described in the last chapter, the $^{20}Ne(d,n)^{21}Na$ experiment was done at reaction energies of 5.16 $\pm$ 0.01 and 6.08 $\pm$ 0.01 MeV, supplementing the work of M.B. Burbank who utilized a reaction energy of 3.92 $\pm$ 0.01 MeV. The machine energy, calibrated using $^{7}Li(p,n)^{7}Be$, $^{13}C(p,n)^{13}N$ and $^{19}F(p,n)^{19}Ne$ thresholds, in the two cases was 5.40 and 6.32 MeV. The mean reaction energy was determined by assuming the ground state Q-value for the $^{20}Ne(d,n)^{21}Na$ reaction to be 0.208 MeV (Ma 66) and using the flight time of the ground state neutron group. The time calibration line for the 6.08 MeV work was determined by doing a $^{9}Be(d,n)^{10}B$ thin target run at 0°, using the known Q-values from Endt and Van der Leun (En 62). A more accurate method was used for the 5.16 MeV work. It involved using the flight time and peak position of the gamma-ray group and finding the slope of the calibration line by means of the electronics setup of fig. 3-1. Since the stop pulses are less frequent than the start pulses, output pulses may result from a start-stop time difference of 1, 2, 3 . . . cycles. The average spacing of the peaks (in channels) is measured to calculate the number of ns. per channel:

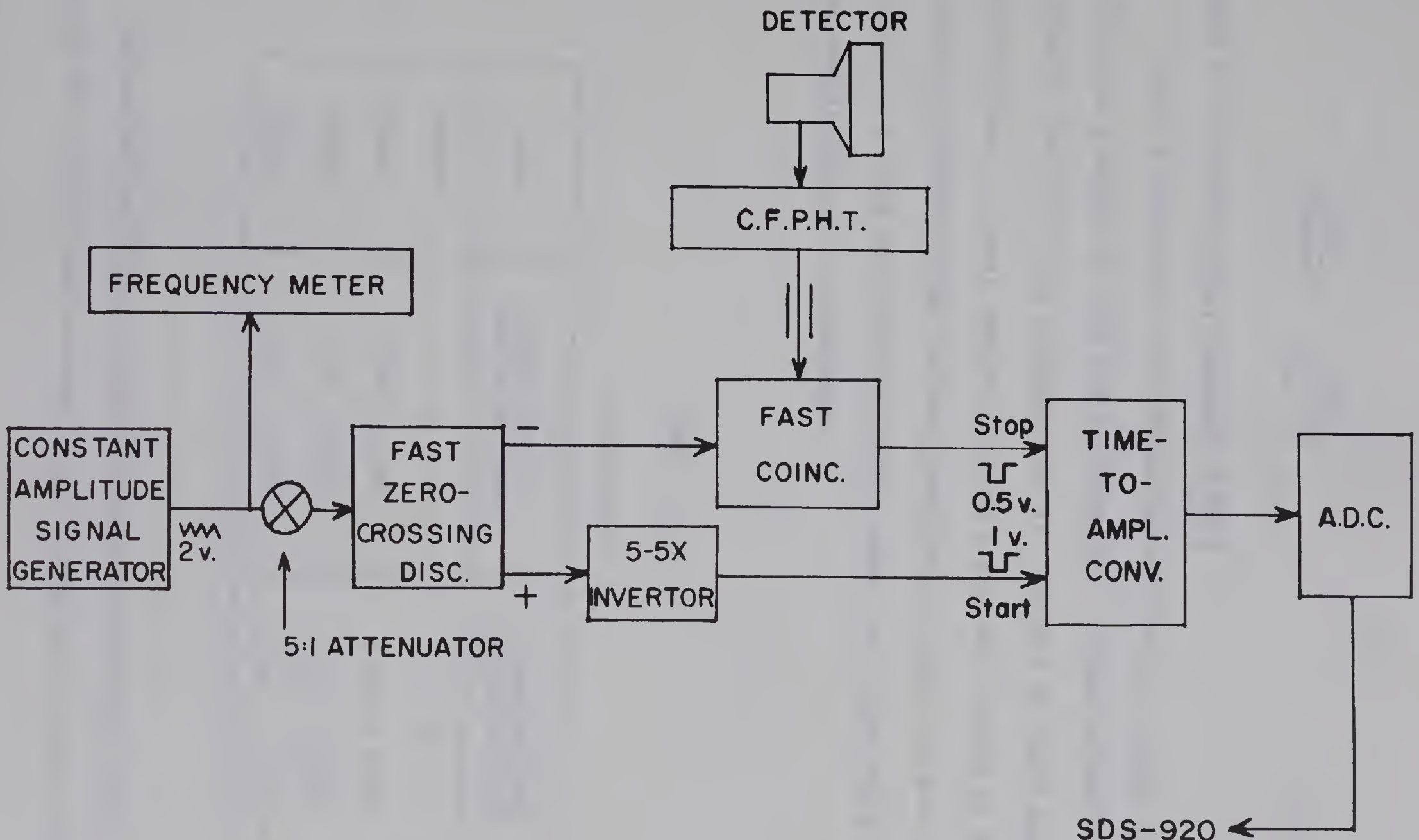

Fig.3-1: Time-calibration Electronics

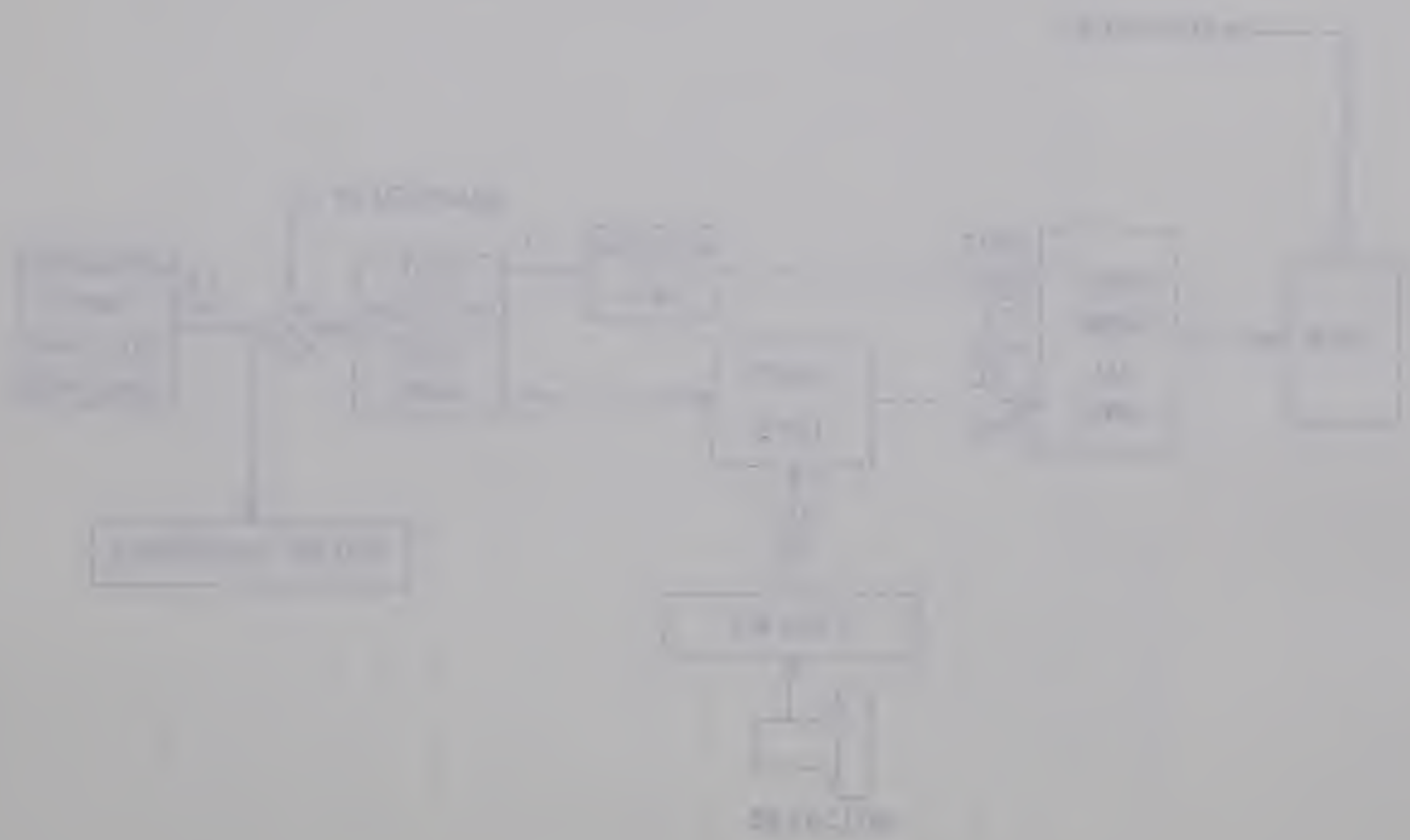

$$\frac{\text{ns.}}{\text{channel}} = \frac{10^3}{\overline{\Delta}_{pp} \cdot f} \qquad (3.1\text{-}1)$$

where f is the oscillator frequency $(\frac{\text{mc.}}{\text{sec.}})$.

With the calibration line determined and reaction energy known, the excitation energies of ^{21}Na can be determined. These excitation energies, listed in table 3-1, are averages over all the runs of the 3 angular distributions. A least squares mass-and-Q program, written by T.B. Grandy, is used to determine from the peak positions, not only the most probable Q-value of a state but the most probable mass, the latter being useful for the identification of contaminants.

TABLE 3-1

Excitations

Level	Experimental Excitation (MeV)	Previous Work Excitation (MeV)
Ground	0	0
First	0.336 ± 0.006	0.338 ± 0.002
Second	1.73 ± 0.02	1.72 ± 0.04
Third	2.43 ± 0.02	2.41 ± 0.01

Our excitation energies compare favorably with those found in previous work (En 67) but are less accurate except in the case of the 1.73 MeV state.

Thus the quoted excitation energies will be those of Endt and van der Leun except for the 1.73 MeV state, which will be ours.

Fig. 3-2 shows a typical time-of-flight spectrum, including the calibration line. The right-hand $^{13}N(0.0)$ and $^{13}N(2.36)$ peaks are due to the presence of carbon on the front collimator; those on the left are due to carbon on the Faraday cup. The ^{17}F groups are due to the presence of oxygen in the gas.

3.2 Resolution Studies : the 2.41 MeV State

Contributing factors in the resolution of the system are:

(1) beam width

Measurements have shown that the intrinsic beam width of the University of Alberta Van de Graaff-Mobley combination for a 6 MeV deuteron is about 0.4 nsec (Mc 67).

(2) scintillator thickness

The flight time of the neutron across the scintillator varies with neutron energy. For neutron energies of 6.0 and 3.5 MeV and a scintillator thickness of 2.0 cm., the times are 0.58 and 0.78 nsec. respectively.

(3) response time of the detection system

The light function of the scintillator, the behavior of the electrons in the photomultiplier and effect of the electronics system contribute under this heading (Mc 67). For neutron energies of 6.0 and 3.5 MeV, the contributions as measured are 0.60 ($\pm$ 0.1) and 0.70 ($\pm$ 0.1) nsec. respectively.

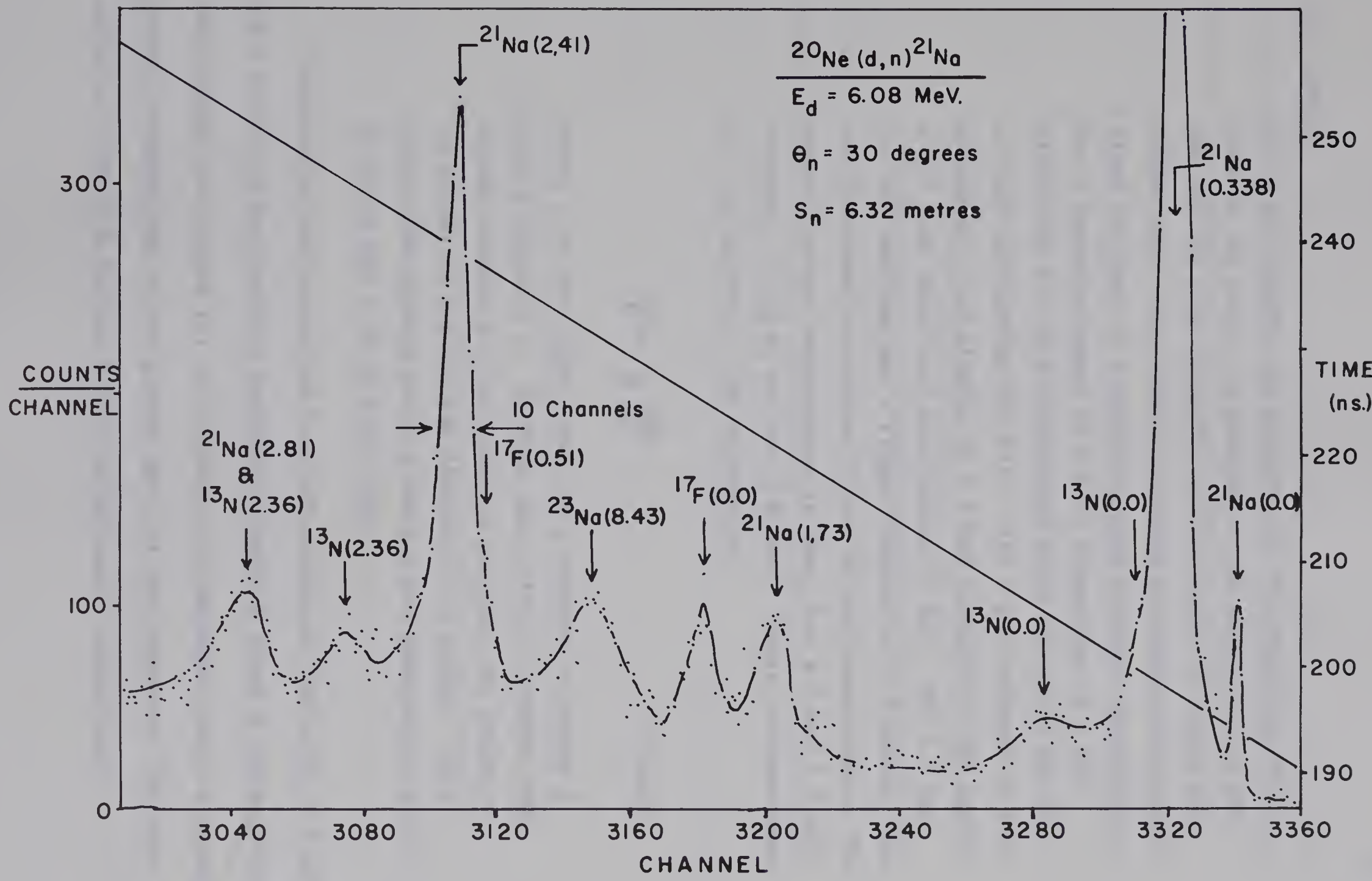

Fig. 3-2: Time-of-Flight Spectrum

(4) target

For a gas target, the factors are the straggling of the beam in the foil, the slowing of the projectile in the gas and the time taken for the projectile to cross the target cell. The first two points are energy uncertainties; the last is a neutron flight distance uncertainty. For a deuteron energy of 6 MeV, straggling in a 100 micro-inch Pt. foil contributes about 40 ($\pm$ 10) keV by a rough calculation (Ev 55). With a gas pressure of 1/4 atmosphere, the slowing of a 6 MeV deuteron in the gas of a 1/2 inch thick cell contributes 27 keV. For 6.0 and 3.5 MeV neutrons and a flight distance of 6.3 metres, the cell thickness contributes 28 and 12 keV respectively. The overall target contribution is then, for 6.0 and 3.5 MeV neutrons, 55 ($\pm$ 8) and 50 ($\pm$ 8) keV. These are converted to time spreads by the expression:

$$\frac{\Delta t}{t} = \frac{1}{2} \frac{\Delta E}{E} \qquad (3.2\text{-}1)$$

where t is the flight time for a neutron of energy E over a distance d. In this case, since a maximum time spread between any two peaks is desired, the detector is placed at the maximum distance, 6.3 metres. This gives time spreads for 6.0 and 3.5 MeV neutrons of 0.87 $\pm$ (0.13) and 1.70 ($\pm$ 0.27) nsec.

Considering the ground and 2.41 MeV states of ^{21}Na at E_d = 6 MeV and θ = 30°, we have neutron energies of about 6.0 and 3.5 MeV. Using the figures from points (1) to (4) above, we estimate that the neutron groups corresponding to the ground and 2.41 MeV states of ^{21}Na have widths of 1.27 ($\pm$ 0.13) and 2.10 ($\pm$ 0.26) nsec. respectively.

In fig. 3-2, we see that the widths of the ground and 2.41 MeV groups are about 4-1/2 (± 1/2) and 10 (± 1/2) channels, which corresponds to time widths of 1.02 (± 0.12) and 2.27 (± 0.12) nsec. Our calculated 1.27 nsec for the ground state group seems to be a slight overestimate although it is just within error. Thus the calculated 2.10 nsec. for the 2.41 MeV state is probably a slight overestimate as well.

It should be noted that the group corresponding to the ^{17}F - 0.51 MeV state falls under the 2.41 MeV peak and represents about 5% of the area. This broadens the peak somewhat. Thus no definite conclusion can be drawn as to the existence of a second ^{21}Ne state near 2.41 MeV.

In the 3.92 MeV work (Bu 67), which had lower background and better resolution to its advantage, the second state was not detected.

3.3 Cross-Sections

Peak areas are extracted using a peak fitting program of J.W. Tepel (Te 66). The program first determines which are the background points by calculating a gradient for each point and throwing out points with gradients that are too large. The background points are then weighted - the largest weights going to the lowest points - and fitted with a straight line or parabola. Finally, peak positions and shapes are determined using an input reference peak and the resultant peak areas are output along with peak-fitting errors. For the ^{21}Na work, the 0.338 MeV

peak at 30 degrees was used as the reference shape for the ground and 0.338 MeV peaks, while the 2.41 MeV peak at 0 degrees was used as the reference shape for the 2.41 MeV peaks. The program failed to fit the 1.73 MeV peaks because of their small size, high background and contaminant peaks. Therefore these peaks were fitted by hand. The 'hand' method, involving the plotting out of the peak and eyeball estimation of the background and peak shape, yielded sums which, for the ground state peaks, were within 5% of the 'Tepel' sums.

The peaks in the gamma-ray part of the spectrum corresponding to neutrons which have been incorrectly identified as gamma-rays are similarly summed and their areas are added to the corresponding areas from the neutron part of the spectrum. To get the relative angular distributions, the resultant areas are corrected for contaminants and divided by the area of the 2.41 MeV peak from the monitor spectrum. This division eliminates the need for possible target thickness or charge collection corrections from run to run. A correction is also made for dead time effects and detector efficiency:

$$\text{RELATIVE CORRECTED AREA} = \frac{A + A_\gamma}{A_m} \cdot K \cdot \frac{m.\ell.t.}{\ell.t.} \cdot \frac{1}{\varepsilon} \qquad (3.3\text{-}1)$$

where A = area of a peak in the neutron spectrum
A_γ = area of the peak in the gamma spectrum
A_m = area of the monitor peak
$m.\ell.t.$ = monitor system live time
$\ell.t.$ = main system live time
ε = relative detector efficiency
K = contaminant correction factor

Contaminant peaks subtracted out were the ^{17}F - 0.51 MeV peak under the 2.41 MeV peak and the ^{13}N ground state peak under the 0.338 MeV peak. The area of the ^{13}N peak was determined by doing a background run to find the ratio of the two ^{13}N ground state peaks, then summing the left-hand ^{13}N ground state peak in the ^{21}Na spectrum. The area of the ^{17}F - 0.51 MeV peak was determined by summing the ^{17}F ground state peak in each spectrum and multiplying by the ratio $\frac{(d\sigma/d\Omega)_{0.51}}{(d\sigma/d\Omega)_{gd.}}$ where these cross-sections have been measured by Yaramis (Ya 61) at E_d = 5.02 MeV. It is assumed that these ratios are good for the 6 MeV work.

The ^{17}F ground state peak area could also be used in determining the amount of air present in the cell during the ^{20}Ne runs.

A single run at 20 degrees was attempted to serve as the absolute normalization for the angular distributions, where the absolute cross-sections are given by:

$$\left(\frac{d\sigma}{d\Omega}\right)_{exp.} = \frac{A'}{nN\Omega\varepsilon_a} \cdot 10^{27} \ \frac{mb}{sr} \qquad (3.3\text{-}2)$$

where $A' = (A + A_\gamma) \ \frac{t.t.}{\ell.t.} \ K$ (counts)

$t.t.$ = true time (sec.)

n = number of deuterons = $\frac{Q}{1.6 \times 10^{-13}}$

Q = true charge (μCoul)

N = number of target nuclei per $cm.^2$

Ω = solid angle subtended by the detector = 1.51×10^{-4} sr. @ 6.3 m.

ε_a = absolute efficiency of the detector

However, it was discovered that the area of a peak was a function of the beam current, meaning that the apparent charge collected was not equal to the true charge due to the beam. This problem, which could have been due to secondary electrons, could not be corrected using the present target set up. The absolute normalization was then accomplished by doing a separate run on oxygen with the same beam current at 5 MeV and 0 degrees and using the known cross-section for the 0.51 MeV state (Ya 61). We have:

$$Q = Q_{meas.} \cdot \frac{(d\sigma/d\Omega)_{meas.,0.51}}{\left(\frac{d\sigma}{d\Omega}\right)_{0.51}} \qquad (3.3\text{-}3)$$

where Q is the true charge and $Q_{meas.}$ is the measured charge. If we replace Q in (3.3-2) by the expression (3.3-3), we see that the absolute efficiency value is now not needed.

This oxygen normalization method also takes care of any effect due to localized heating of the gas as well as the in-and out-scattering of neutrons at 20° due to the cell and surroundings.

The absolute cross-sections for the bound states of ^{21}Na are given in tables 3-2 to 3-5. The group corresponding to the 2.81 MeV state of ^{21}Na was seen but could not be accurately summed due to background. An accurate Q-value could not be obtained for this state. Cross-sections and angles have been changed from the laboratory system to the centre-of-mass system using the Relativistic Kinematics program written by T.B. Grandy (Gr 67).

TABLE 3-2

Ground State Cross Sections

E_d = 5.16 MeV			E_d = 6.08 MeV		
$\theta_{c.m.}$ (deg.)	$\left(\frac{d\sigma}{d\Omega}\right)_{c.m.}$	% Error	$\theta_{c.m.}$ (deg.)	$\left(\frac{d\sigma}{d\Omega}\right)_{c.m.}$	% Error
0.0	0.850 $\frac{mb}{sr}$	17.5	0.0	0.222 $\frac{mb}{sr}$	22.7
5.34	0.720	18.0	5.34	0.178	21.2
10.68	0.600	18.6	10.68	0.275	18.9
16.01	0.620	18.6	16.02	0.242	21.2
21.34	0.450	19.8	21.34	0.377	19.8
26.65	0.380	20.0	26.66	0.521	16.0
31.96	0.340	21.2	31.96	0.470	16.8
37.24	0.365	20.2	37.25	0.560	16.6
42.51	0.388	20.0	42.53	0.512	19.2
47.77	0.330	22.7	47.78	0.415	18.6
53.00	0.355	21.2	53.01	0.348	17.5
58.20	0.410	20.0	58.22	0.249	21.2
63.39	0.478	19.8	63.40	0.216	19.8
73.68	0.458	19.8	73.69	0.308	21.2
83.85	0.500	19.8	83.87	0.364	21.2
93.91	0.608	19.5	93.93	0.504	16.8
108.78	0.660	18.6	108.79	0.385	21.2
123.39	0.730	18.6	123.40	0.435	17.0
137.76	0.868	18.0			
0.0	0.794	17.5			

TABLE 3-3

First Excited State Cross Sections

E_d = 5.16 MeV			E_d = 6.08 MeV		
$\theta_{c.m.}$ (deg.)	$\left(\frac{d\sigma}{d\Omega}\right)_{c.m.}$	% Error	$\theta_{c.m.}$ (deg.)	$\left(\frac{d\sigma}{d\Omega}\right)_{c.m.}$	% Error
0.0	1.81 $\frac{mb}{sr}$	16.5	0.0	1.30 $\frac{mb}{sr}$	16.0
5.35	1.93	16.6	5.35	1.52	15.8
10.70	2.73	16.6	10.70	-	-
16.05	3.75	16.2	16.05	4.36	16.0
21.39	5.64	16.2	21.38	5.93	16.2
26.71	7.46	16.1	26.71	9.68	15.9
32.03	8.15	16.1	32.02	8.39	16.0
37.32	8.30	16.1	37.32	7.81	15.9
42.60	8.20	16.1	42.60	6.51	16.0
47.87	7.10	16.1	47.86	5.93	16.0
53.10	5.78	16.2	53.10	4.24	16.0
58.32	4.58	16.2	58.32	2.67	16.0
63.51	3.27	16.6	63.51	1.65	16.8
73.81	1.71	16.6	73.80	1.02	16.2
83.99	0.98	17.5	83.99	0.63	16.2
94.05	1.04	17.5	94.05	1.03	16.4
108.91	1.11	17.5	108.91	1.22	16.2
123.51	1.12	17.2	123.50	1.17	16.4
137.86	1.06	17.5			
0.0	1.41	17.0			

TABLE 3-4

Second Excited State Cross Sections

E_d = 5.16 MeV		
$\theta_{c.m.}$ (deg.)	$\left(\frac{d\sigma}{d\Omega}\right)_{c.m.}\left(\frac{mb}{sr}\right)$	% Error
0.0	0.308	25
5.42	0.300	25
10.84	0.365	25
16.25	0.332	25
21.66	0.418	25
27.05	0.455	25
32.42	0.439	25
37.78	0.392	25
43.12	0.378	25
48.43	0.453	25
53.71	0.457	25
58.97	0.486	25
64.20	0.445	25
74.56	0.345	25
84.78	0.389	25
94.85	0.379	25
109.68	0.403	25
124.20	0.309	25
138.43	0.313	25
0.0	0.270	25

TABLE 3-5

Third Excited State Cross Sections

E_d = 5.16 MeV			E_d = 6.08 MeV		
$\theta_{c.m.}$ (deg.)	$\left(\frac{d\sigma}{d\Omega}\right)_{c.m.}\left(\frac{mb}{sr}\right)$	% Error	$\theta_{c.m.}$ (deg.)	$\left(\frac{d\sigma}{d\Omega}\right)_{c.m.}\left(\frac{mb}{sr}\right)$	% Error
0.0	61.10	15.8	0.0	62.20	15.8
5.48	55.35	15.8	5.45	60.30	15.8
10.95	44.10	15.9	10.89	45.30	15.9
16.42	30.45	15.9	16.33	26.80	16.0
21.88	17.95	16.0	21.76	10.64	15.9
27.32	8.05	16.0	27.18	4.96	15.9
32.74	3.66	16.2	32.58	2.33	18.6
38.15	2.17	16.6	37.96	-	-
43.53	2.57	16.6	43.31	2.57	16.0
48.88	3.82	16.2	48.64	4.04	15.9
54.20	5.03	16.2	53.95	-	-
59.49	5.57	16.2	59.22	4.66	16.0
64.75	5.57	16.2	64.46	3.56	16.0
75.16	4.90	16.2	74.84	3.13	16.2
85.40	3.91	16.2	85.08	1.77	16.2
95.49	2.92	16.6	95.16	1.44	16.2
110.30	2.07	16.6	109.98	1.07	16.6
124.75	1.70	16.6	124.46	1.06	16.2
138.88	1.66	16.6	138.64	-	-
0.0	62.30	15.8	0.0	60.80	15.8

3.4 Error

The major source of error is that of the normalization to the $^{16}O(d,n)^{17}F$ cross-section, 15%. Other errors coming into play are the peak-fitting errors and the uncertainty in the number of ^{20}Ne nuclei present due to the presence of air in the cell. The peak fitting error varies from peak to peak while the ^{20}Ne uncertainty is about 5%. All other errors are negligible. A rough calculation showed that the effect of the in-and out-scattering of the neutrons for angles from 0 to 135 degrees was less than 1/2%.

The 1.73 MeV peak error is large due to the relatively large background. The estimated summing error is about 20% for this peak.

3.5 Excitation Curves

An excitation curve was attempted for each state of ^{21}Na except the 1.73 MeV state, from 4.0 to 6.3 MeV in steps of 50 keV, at 20 degrees. Because of the charge collection difficulty, the results are not very accurate. A rough correction was made by varying the beam and plotting a given peak's area against the average beam current. For each run of the excitation curves, the average beam current was noted and a correction factor thus applied to the points of the excitation curves. The fluctuations in the corrected curves were less than 15% for the 2.41 MeV and 0.338 MeV states, meaning that resonance and interference effects may not be too important for these states from 4.0 to 6.3 MeV. The ground state excitation curve was mostly flat except for a large peak near E_d = 4.3 MeV.

CHAPTER IV

DWBA AND HAUSER-FESHBACH THEORIES

4.1 Application

The Distorted-Wave Born Approximation (DWBA) theory and Hauser-Feshbach (HF) theory are used to calculate (d,n) cross-sections which are compared to the experimental cross-sections. The stripping angular distributions are generated using the DWBA program written by P.D. Kunz (Ku 67a). The DWBA theory is given in Appendix I. A Woods-Saxon optical potential with zero volume absorption is employed, using the local, zero-range approximation. Table 4-1 lists the parameters. The neutron parameters are those given by Perey and Buck (Ro 66) while those for the deuteron are obtained from fits of elastic scattering data at 10.95 and 11.6 MeV (Bu 67). In the latter work, a potential set was chosen for which the real well depth is equal to the sum of the real depths for the neutron and proton ($\approx$ 100 MeV). The parameters for the bound proton are r_0 = 1.25 fm. and a = 0.65 fm. The program adjusts V for the bound proton until the correct binding energy is attained.

Hauser-Feshbach theory uses a statistical approach to estimate the cross-sections for the formation of the compound nucleus. Appendix II gives the HF theory. A program written by W.R. Smith (Sm 65) and modified by N. Davison (Da 68) to include the level density formulae is

TABLE 4-1

Optical Model Parameters

	Deuteron	Neutron	Alpha
$-V$ (MeV)	95.0	48.0-0.29E	125.0
W_D (MeV)	102.8	38.4	30.0
$-V_S$ (MeV)	0	28.8	0
W_S (MeV)	0	0	0
r_0 (fm)	1.228	1.27	1.9
r_0' (fm)	1.291	1.27	1.9
a (fm)	0.671	0.66	0.55
a' (fm)	0.625	0.47	0.55
r_C (fm)	1.3		1.9

TABLE 4-2

Level Density Parameters

Reaction Channel	Q(MeV)	a	$b(MeV^{-\frac{1}{2}})$	E_{Beg}(MeV)
$^{20}Ne(d,d)^{20}Ne$	--	- 0.96	0.725	7.0
$(d,n)^{21}Na$	+ 0.208	- 0.57	0.75	3.6
$(d,p)^{21}Ne$	+ 4.535	- 0.78	0.87	3.8
$(d,\alpha)^{18}F$	+ 2.797	- 0.15	0.65	3.1

used. Required data include:

(1) the optical model parameters corresponding to the open channels which are the (d,n), (d,p), (d,α) and (d,d) channels. (See table 4-1). The α-parameters have been chosen arbitrarily since no appropriate data for α-scattering is available. The proton parameters have been taken to be the same as those for the neutron, with r_c = 1.3 fm.

(2) the Q-values and spin-parities for the known levels that may be excited in the residual nuclei. These are taken from Endt and van der Leun (En 67) (En 62) and Pronko (Pr 67).

(3) the values of 'a' and 'b' of the level density expression (App. II) for each residual nucleus. These are determined by fitting a straight line to plotted values of $\log_{10} N(E_x)$ versus $E_x^{1/2}$ where $N(E_x)$ is the number of levels with excitation energies less than E_x.

Table 4-2 lists the values of 'a' and 'b', $E_{beg.}$ - the excitation energies above which the level densities are used-and the ground state Q-values of the reactions.

The resultant (d,n) cross-sections are found to be rather insensitive to reasonable variations in 'a' and 'b', the optical model parameters for the alpha-particle and proton and the value of σ (App. II).

Figs. 4-1 to 4-4 show the results of the DWBA and HF calculations along with the experimental points and their absolute errors. The spectroscopic factors, S, are determined from the relation:

$$\left(\frac{d\sigma}{d\Omega}\right)_{exp.} = \left(\frac{d\sigma}{d\Omega}\right)_{HF} + S\left(\frac{d\sigma}{d\Omega}\right)_{DWBA} \qquad (4.1\text{-}1)$$

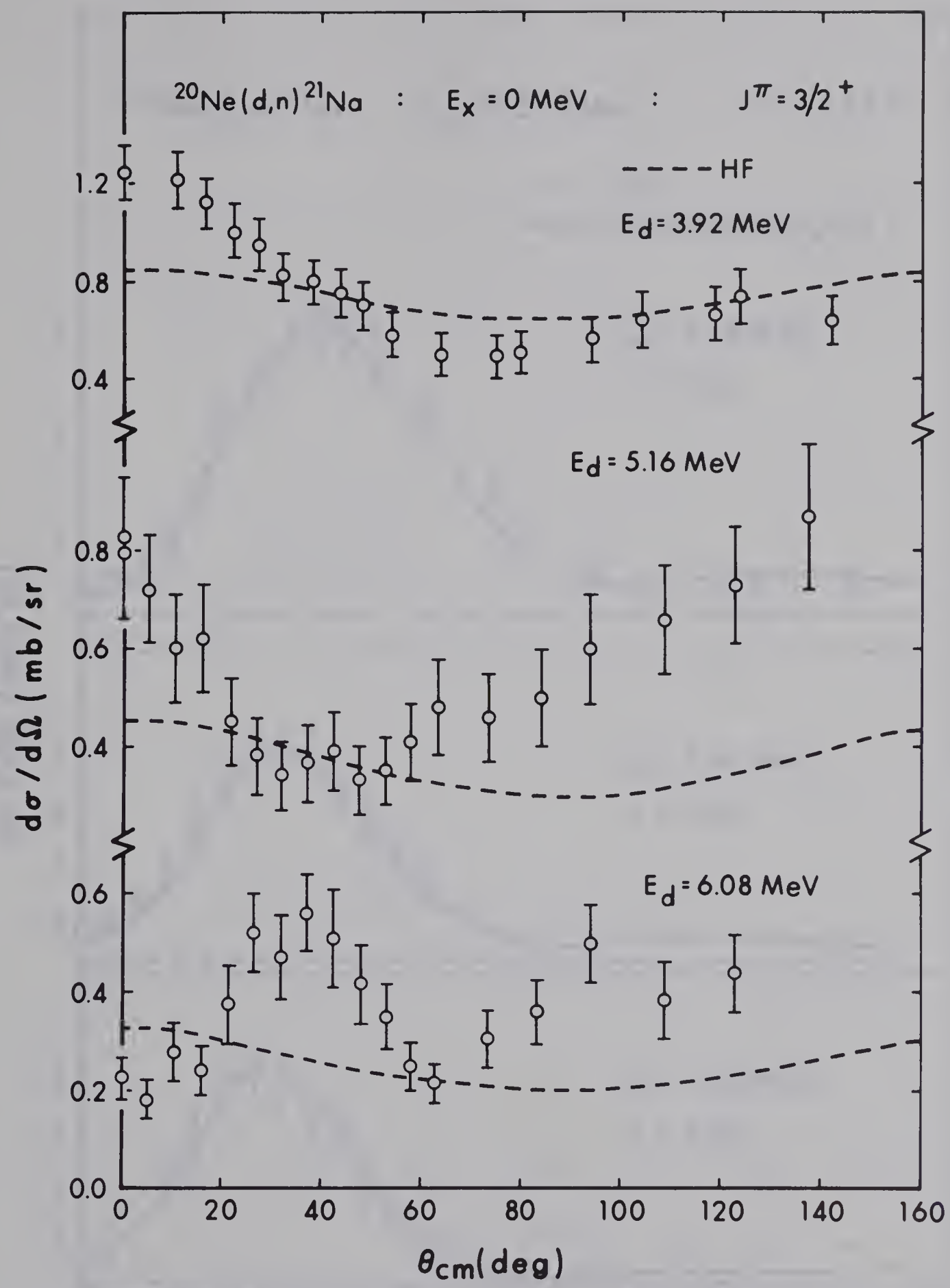

Fig.4—1:Ground State

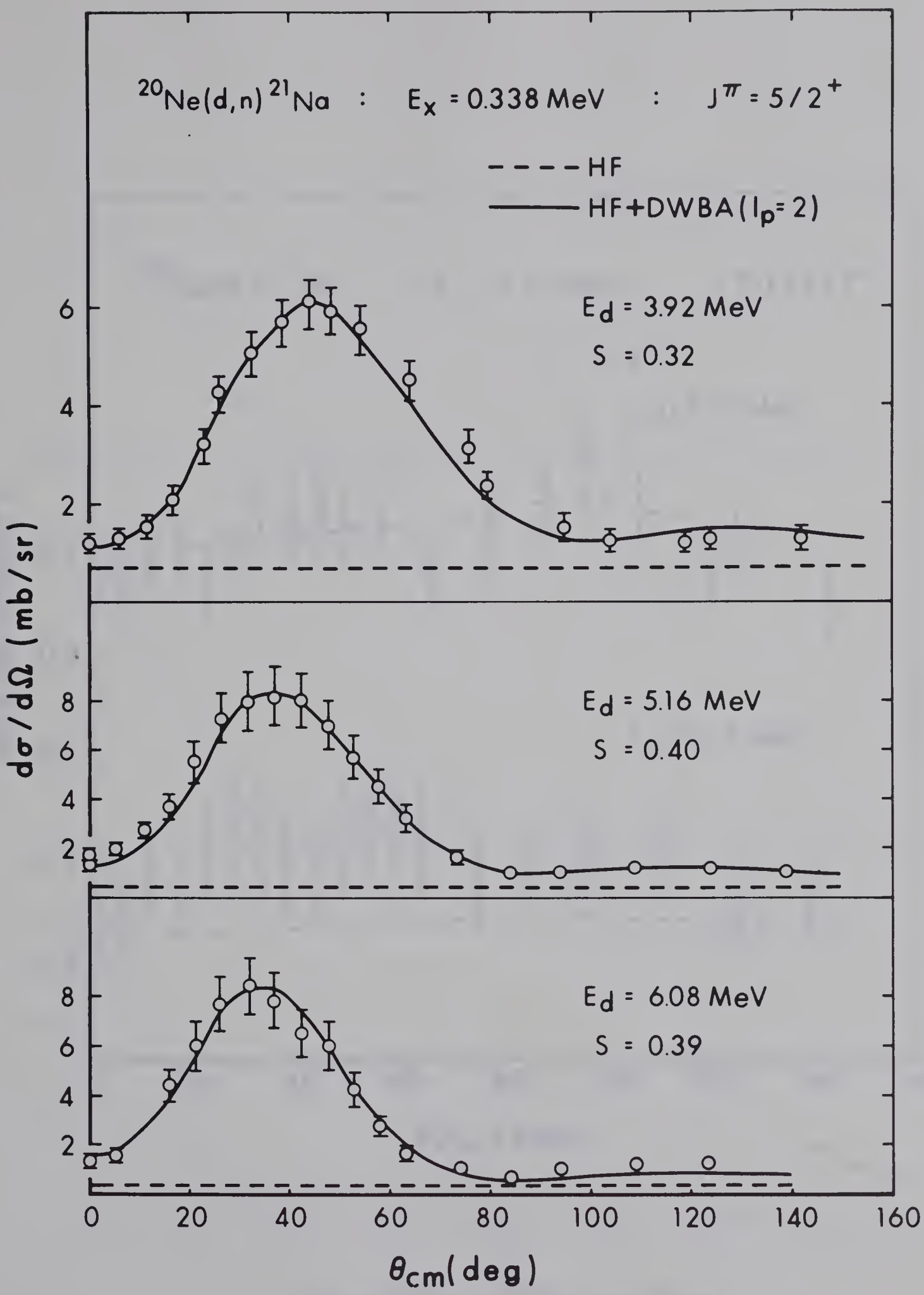

Fig.4—2:First Excited State

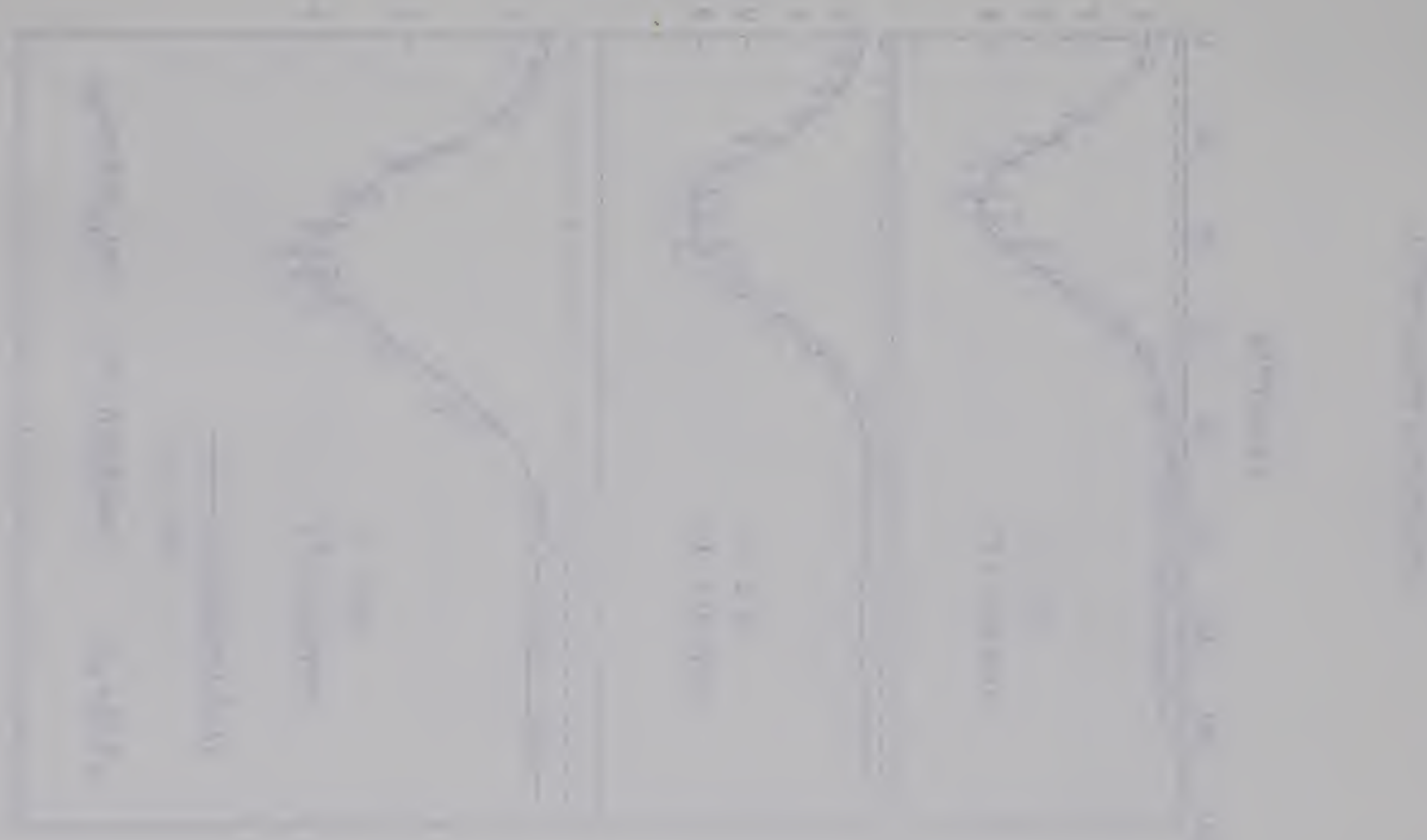

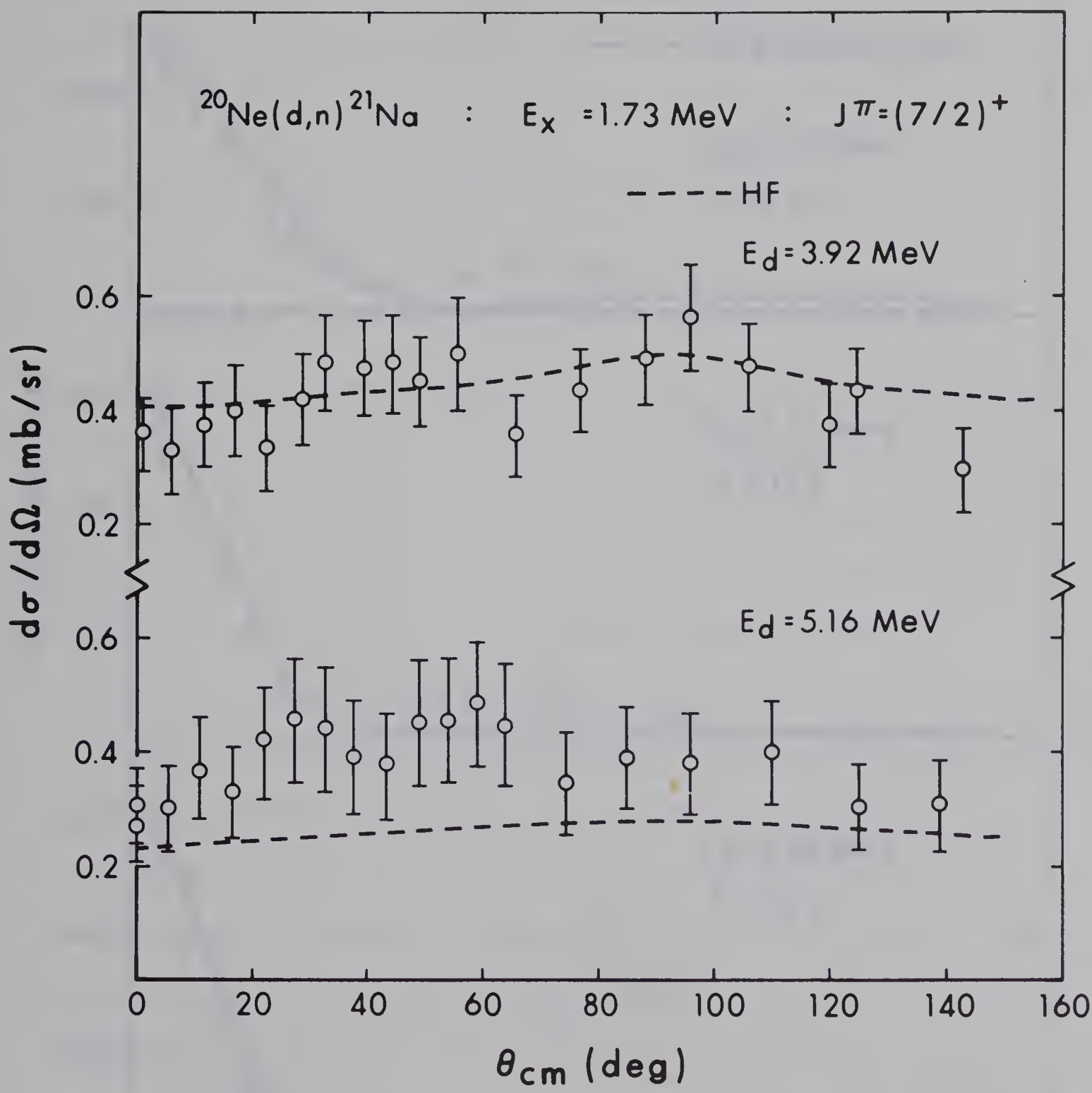

Fig.4—3:Second Excited State

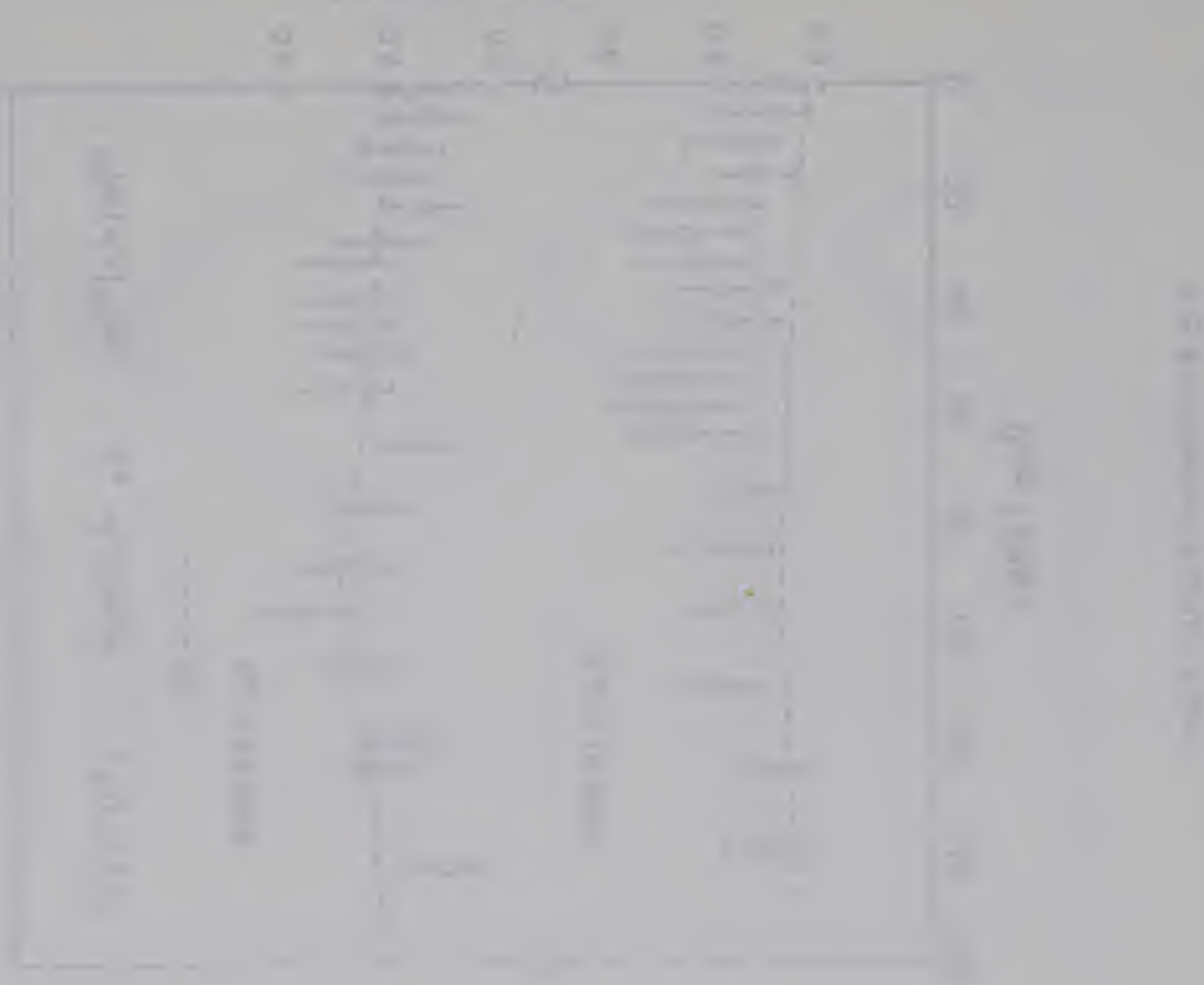

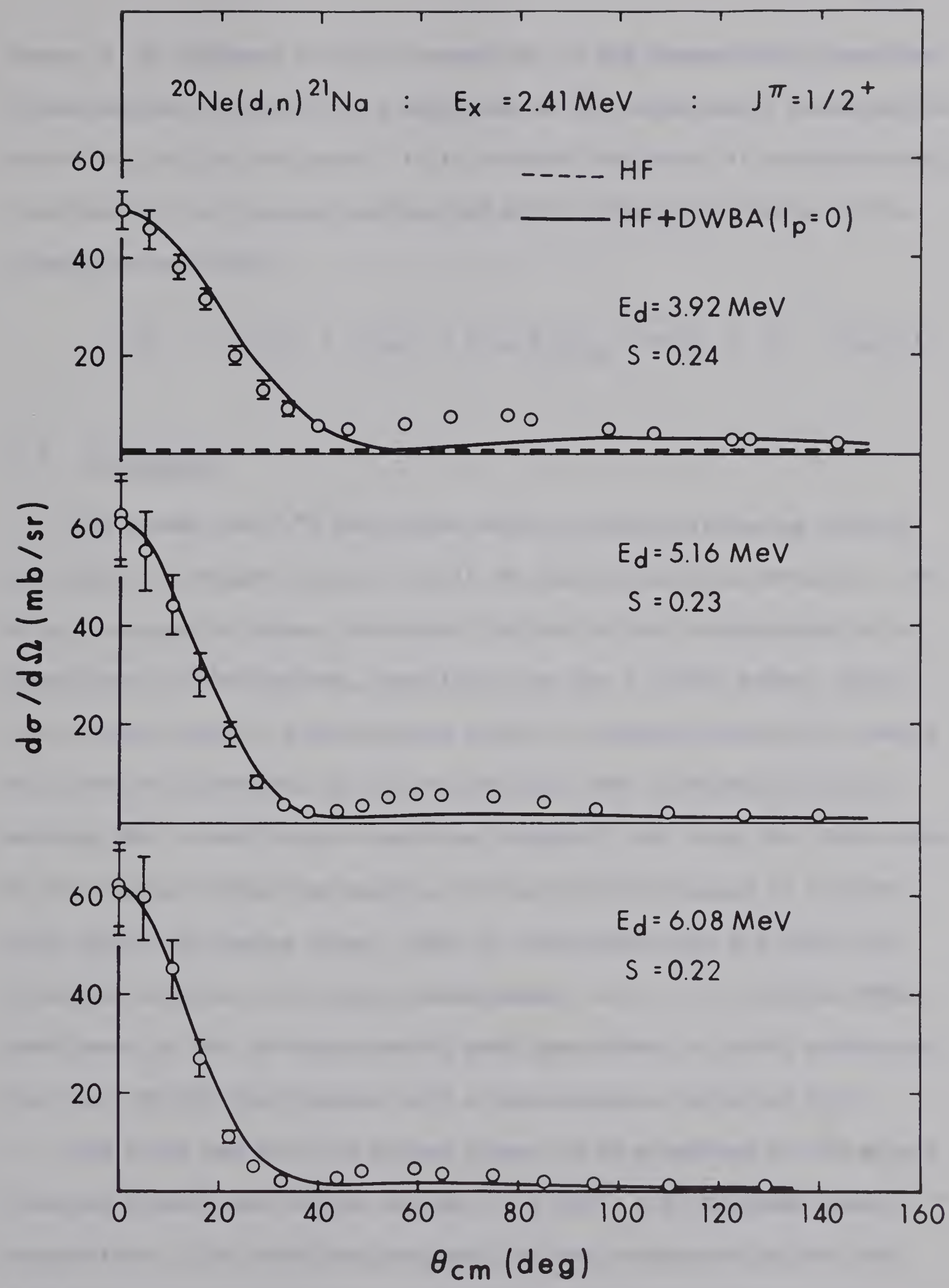

Fig.4—4 : Third Excited State

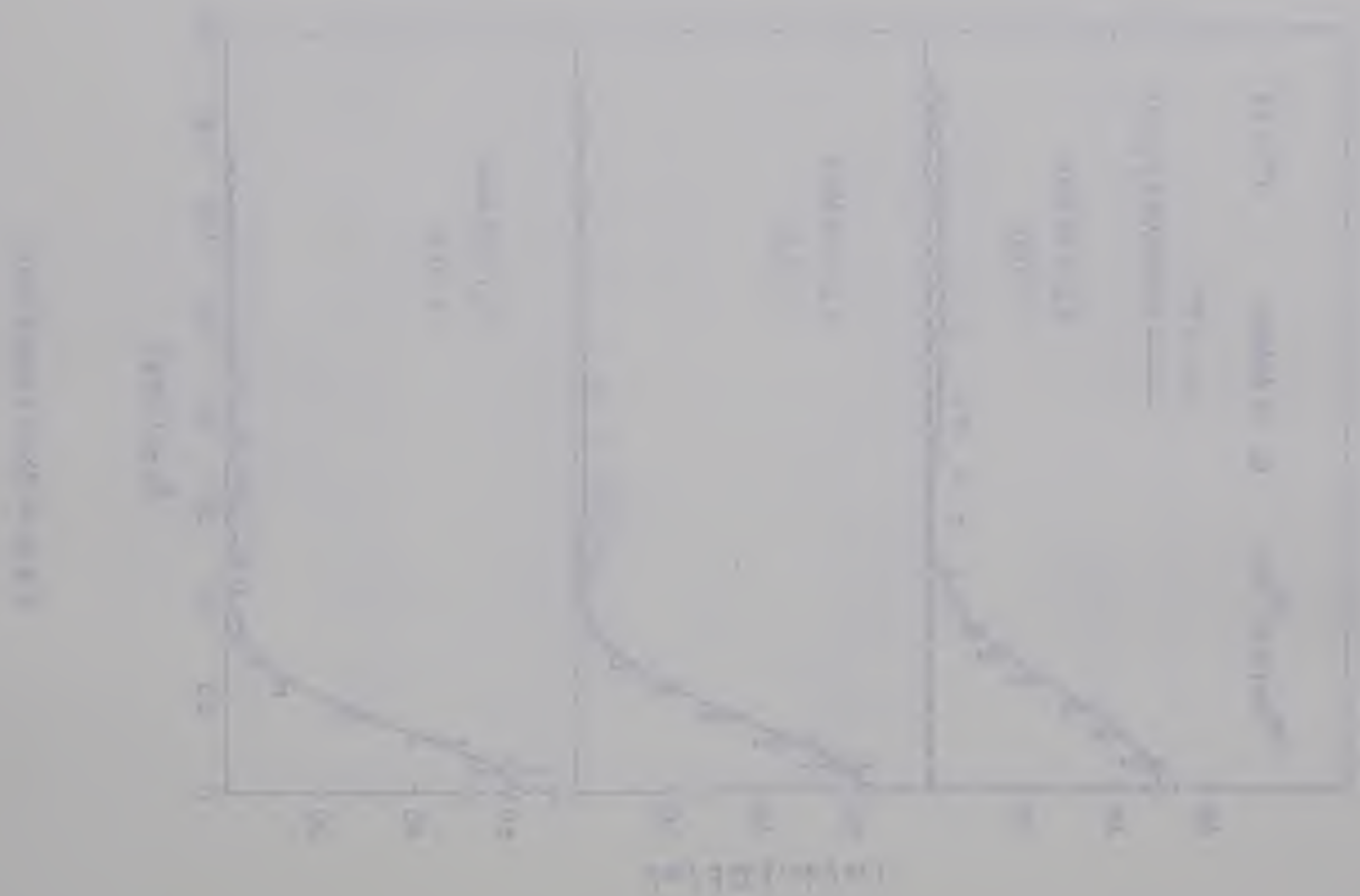

where S is adjusted until the magnitude of the theoretically predicted cross-section is equal to the magnitude of the experimental cross-section at the top of the main peak. It is assumed that there is no interference term between the compound nucleus and direct interaction parts of the transition amplitude:

$$|T|^2 = |T_{DI}|^2 + |T_{CN}|^2 + \cos\phi\ T_{DI}T_{CN}\ ;\ \cos\phi = 0 \qquad (4.1\text{-}2)$$

4.2 Discussion

The ground and 1.73 MeV states show no typical stripping pattern and hence are thought to be a result of compound nucleus formation. The HF predictions for these two states lie very close in magnitude to the experimental distributions, especially for the 1.73 MeV state. The ground state angular distributions exhibit a changing shape with energy which may be attributed to the interference term in equation (4.1-2) meaning that a small direct reaction component may exist for this state. At the highest bombarding energy, the distribution begins to take on a more typical stripping shape, which is consistent with the idea that at higher energies, stripping predominates. An $\ell = 2$ - transfer DWBA peak seems to fit the experimental peak when added to the HF prediction for the 6.08 MeV distribution with a spectroscopic factor of 0.02.

The 0.338 and 2.41 MeV states appear to be populated by the direct reaction channel and exhibit strong $\ell = 2$ and $\ell = 0$ stripping peaks respectively. The predicted compound nucleus cross-sections for the 2.41 MeV state are relatively negligible. For the 0.338 MeV state,

they modify the spectroscopic factors to a small extent. The resulting spectroscopic factors for the 2.41 MeV state are consistent for the 3 bombarding energies; those for the 0.338 MeV state differ somewhat which may partly be a result of the contaminant group under the peak for the 0.338 MeV level for the 5.16 and 6.08 MeV work.

In the Shell Model description, one can see why the stripping cross-sections are enhanced for two of the states and reduced for the other two. The 0.338 MeV state ($5/2^+$) is populated by putting the single protons in the $1d_{\frac{5}{2}}$ shell while the 2.41 MeV state ($1/2^+$) is populated by putting the single protons in the $2s_{\frac{1}{2}}$ shell. A small $1d_{\frac{3}{2}}$ component may be present accounting for the small cross-sections for stripping to the ground state ($3/2^+$), but a final spin of $7/2^+$ is impossible for single particle stripping in the s-d shell accounting for zero stripping amplitude for the 1.73 MeV state ($7/2^+$).

It is interesting to find out how sensitive the spectroscopic factors are to changes in some of the optical model parameters and the incorporation of finite range and nonlocality approximations in the stripping calculation. Table 4-3 lists the variations in S at E_d = 6.08 MeV. S seems not to be very sensitive to spin-orbit effects, binding energy variations, the finite range addition or even a large change in the imaginary well depth of the deuteron. The addition of nonlocality creates an appreciable change but it should be noted that its incorporation is only an approximation (see App. I). We can thus see that although the deuteron optical parameters are obtained from data at a bombarding energy much higher than that used in the present

TABLE 4-3

Sensitivity of the Spectroscopic Factors to the Form and Parameters of the DWBA Calculation

Change in Optical Model Parameters	Variation in S for the 0.338 MeV State (E_d = 6.08 MeV)	Variation in S for the 2.41 MeV State (E_d = 6.08 MeV)
No spin-orbit for the neutron	- 0.5%	- 3.0%
With spin-orbit for the deuteron (V_S = -15 MeV)	+ 0.5%	0.0%
With spin-orbit for the proton (V_S = -30 MeV)	- 8.5%	0.0%
With (W_D = 60 MeV)	- 8.5%	- 2.5%
With 0.03 MeV subtracted from the binding energy	- 1.5%	- 1.5%
With finite range†	- 2.5%	- 3.5%
With nonlocality††	- 22.0%	- 13.0%

† $\beta^{-1} = 0.65$ fm .

†† $\beta_p = \beta_n = 0.85$ fm; $\beta_d = 0.54$ fm .

experiment, the resultant spectroscopic factors should not be greatly affected by this.

The overall results are dependent upon the approximations made in the DWBA theory, which are:

(1) V is a central force and equal to V_{pn}.

(2) the D-state of the deuteron is ignored.

(3) only first-order perturbation theory is used.

(4) the radial wave functions are solutions of a spherically symmetric potential whereas ^{21}Na is known to be a deformed nucleus.

However, the overall features of the data are reproduced by the model to such a good extent that these approximations appear to be good.

CHAPTER V

THE NILSSON MODEL

5.1 Introduction

The strong coupling collective (Nilsson) model has had good success for nuclei in the s-d shell, particularly those with mass 25 (Li 58). A number of groups have applied the model to ^{21}Ne (Pr 67, Pe 65a, Ho 65a, Fr 60, Ho 67) and ^{23}Na (La 65, Br 62, Ha 64, Pa 58, Cl 62, Gl 64) with apparent success. ^{21}Na has not been studied as much on account of the lack of experimental data.

The majority of papers have only a comparison of the theoretical and experimental level schemes. Fig. 5-1 shows the level schemes of ^{21}Na, ^{21}Ne, ^{23}Na and ^{23}Mg. They are very similar in the region of low-lying excitation - the dashed lines show possible correspondences between levels of similar nature. Each nucleus can be described as an even-even core coupled to a single nucleon so that the model should apply equally well to each one. Pelte and Povh (Pe 65a) and Pronko (Pr 67) give good discussions of the collective model and the level scheme of ^{21}Ne. Lancman (La 65) has done a 4-band Rotational-Particle Coupling (RPC) calculation for ^{23}Na in which theoretical level positions and the $C_{K\alpha}$ coefficients (see App. III) are given. Benenson and Lidofsky (Be 61) include a 3-band calculation with RPC for ^{21}Na in which reduced widths are calculated which are in qualitative agreement with those found

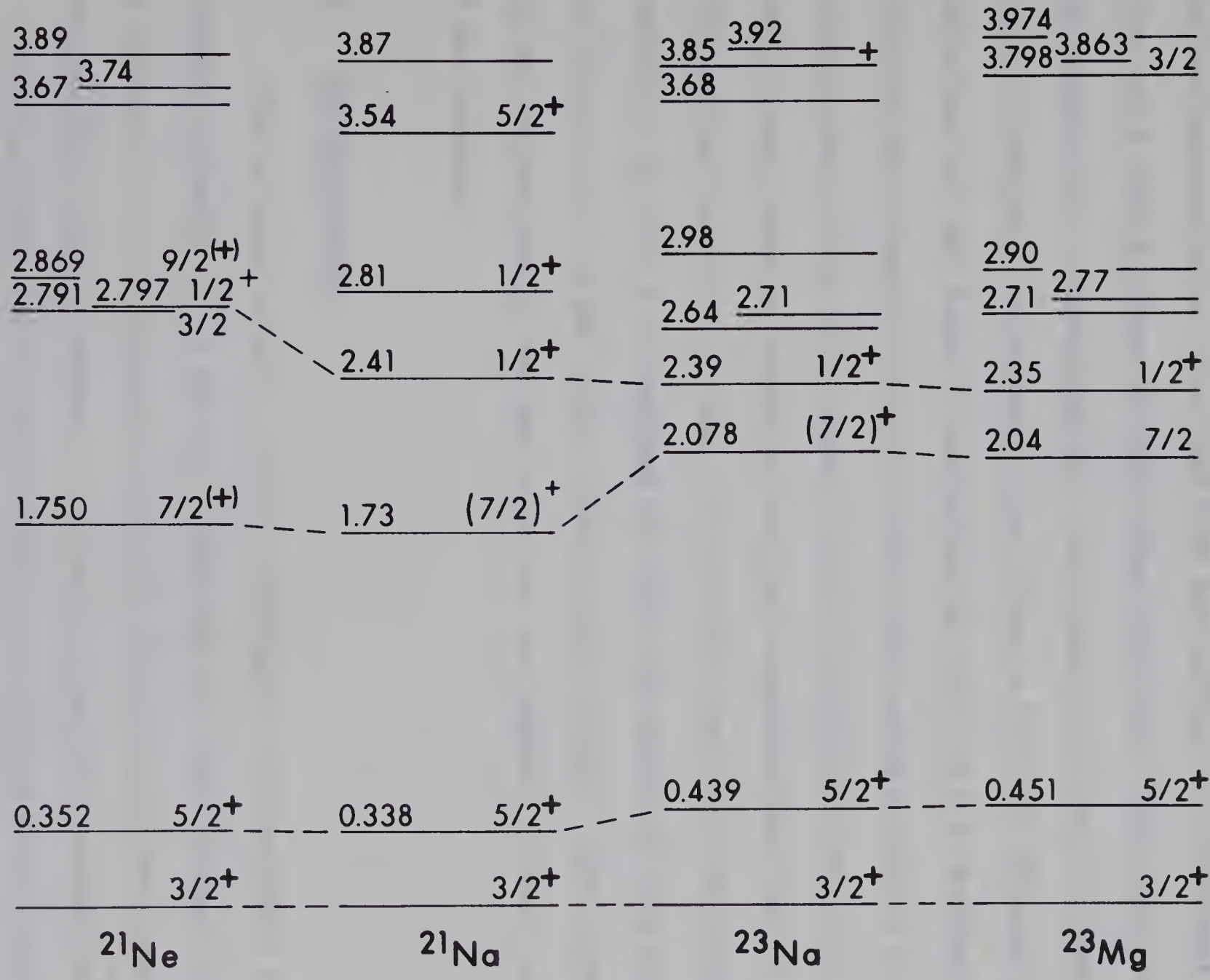

Fig.5–1: Level Diagrams

experimentally, although the ground and 0.338 MeV states could not be resolved experimentally.

The Nilsson Model, including RPC, is applied to ^{21}Na assuming the nucleus consists of an even-even ^{20}Ne core giving the rotational contribution and a single proton in orbit about this core. The theory is given in Appendix III. Neglecting RPC, the ground, 0.338 and 1.73 MeV levels can be interpreted as members of the $|K\pi\alpha\rangle = |3/2 + 7\rangle$ Nilsson band, while the 2.41 MeV level is interpreted as the $|1/2 + 9\rangle$ bandhead. Although the evidence for the 2.81 MeV state having a spin of 1/2 is rather weak (Aj 61), it is taken to be the bandhead of the $|1/2 + 6\rangle$ 'hole' band, which is formed by exciting a particle from the $\alpha = 6$ Nilsson band to the $\alpha = 7$ band. The 3.74 MeV level of ^{21}Ne is interpreted as the $|5/2 + 5\rangle$ bandhead (Ho 65a); the analog of this state in ^{21}Na is the 3.54 MeV level. Thus we have 4 bands. Upon introduction of RPC, states having the same spin that are members of bands with $\Delta K = 1$ mix together.

5.2 The Calculation

^{21}Na is known to have a prolate deformation corresponding to a Nilsson parameter $\eta = 4$ (Ho 65). Regarding the other Nilsson parameters, a choice of $\mu = 0$ is consistent with the Nilsson value for states having the principal quantum number $N \leq 2$, and a spin-orbit interaction strength $\kappa = 0.10$ is chosen from considerations of the ground state properties (Ho 65). Finally, the moment of inertia parameter $\frac{\hbar^2}{2\mathcal{I}}$ is known to be in the region 0.19 to 0.25 MeV for the ground state band (Ke 64, G1 64).

It is chosen to be 0.21 MeV for all 4 bands in the present calculation.

Using the above parameters, the normalized Nilsson wave function coefficients $a_{\ell\Lambda}$ and the numbers r(NKα) (see Appendix III) can be obtained from Nilsson (Ni 55). Then from equations (9) and (12) of Appendix III, the expansion coefficients $\langle N\ell j|K\pi\alpha\rangle$ and bandhead energies $E_0(NK\alpha)$ can be calculated. In order to achieve a better energy level fit, these bandhead energies are varied from their Nilsson values. Table 5-1 lists the bands, their Nilsson and revised bandhead energies, the decoupling parameters as calculated from equation (A.3-11) and the estimates of U_α^2. U_α^2 for the ground state band is taken to be 0.5 (i.e. there is probability 1/2 that the ground state is empty). The 2.41 and 3.54 MeV states, as states of rather high excitation, would correspond to a high probability of being empty. The 2.81 MeV state, a 'hole' state, has a low probability of being empty. The U_α^2 estimates are in accord with those given by Lutz (Lu 67) for ^{23}Ne.

TABLE 5-1

Nilsson Model Parameters

Kπα	$E_0(NK\alpha)$	$E_0'(NK\alpha)$	a	U_α^2
$\frac{3}{2}$ + 7	0 MeV	0 MeV	-	0.5
$\frac{1}{2}$ + 9	2.93	2.06	0.141	0.9
$\frac{1}{2}$ + 6	3.59	2.87	2.107	0.1
$\frac{5}{2}$ + 5	3.94	3.98	-	1.0

TABLE 5-2

The $C_{K\alpha}$ Coefficients

Level		$C_{K\alpha}$			
$J\pi$	$K\pi\alpha$	$C_{\frac{3}{2}\,7}$	$C_{\frac{1}{2}\,6}$	$C_{\frac{1}{2}\,9}$	$C_{\frac{5}{2}\,5}$
$\frac{1+}{2}$	$\frac{1}{2}$ + 6	-	1	0	-
	$\frac{1}{2}$ + 9	-	0	1	-
$\frac{3+}{2}$	$\frac{3}{2}$ + 7	.980	.159	-.117	-
	$\frac{1}{2}$ + 6	-.164	.986	-.035	-
	$\frac{1}{2}$ + 9	.110	.053	.993	-
$\frac{5+}{2}$	$\frac{3}{2}$ + 7	.897	.358	-.152	.210
	$\frac{1}{2}$ + 6	.420	-.614	.587	-.320
	$\frac{1}{2}$ + 9	-.137	.539	.795	.243
	$\frac{5}{2}$ + 5	-.024	-.452	.029	.891

The energies of the unperturbed states can now be calculated (equation A.3-10) as can the off-diagonal elements (equation A.3-14, A.3-15) modified for pairing. Upon diagonalization of the Hamiltonian matrix, we get the energy eigenvalues and the values of $C_{K\alpha}$ (equation A.3-16) (see table 5-2). The latter are used in (A.3-17) to calculate the spectroscopic factors for the states of ^{21}Na. Table 5-3 shows a comparison between the theoretical and experimental spectroscopic factors and level excitations.

5.3 Discussion

The agreement between spectroscopic factors determined from experimental data and those from the Nilsson model is very good for the 4 bound states of ^{21}Na. The theoretical positive parity level excitations correspond quite well to those found experimentally for E_x less than 5 MeV. Fitting the excitation levels by variation of some of the parameters could not be attempted because of the large number of parameters involved and the lack of experimental evidence for the higher levels.

According to the theoretical prediction, the 2.81 MeV state may correspond to the $9/2^+$ member of the ground state band. The $3/2^+$ member of the $\alpha = 9$ band falls near 3.2 MeV and may also correspond to the 2.81 MeV state. Further experimental evidence is needed to pin down the spin-parity of the 2.81 MeV state as $1/2^+$, $3/2^+$ or $9/2^+$. The 3.87 MeV level has no experimental spin-parity, but it could correspond either to the

TABLE 5-3

Comparison of Spectroscopic Factors and Excitations

Experiment			Nilsson Model			Shell Model		
J	E_x(MeV)	$\overline{S}$	J	E_x(MeV)	S	J	E_x(MeV)	S
$\frac{3}{2}$	0	0	$\frac{3}{2}$	0	0.003	$\frac{3}{2}$	0	0.009
$\frac{5}{2}$	0.338	0.37	$\frac{5}{2}$	0.44	0.327	$\frac{5}{2}$	0.46	0.31
$\frac{7}{2}$	1.73	0	$\frac{7}{2}$	1.68	0	$\frac{7}{2}$	-	0
$\frac{1}{2}$	2.41	0.23	$\frac{1}{2}$	2.41	0.252	$\frac{1}{2}$	2.04	0.32
$\left(\frac{1}{2}\right)$	2.81		$\frac{1}{2}$	2.81	0.022			
			$\frac{3}{2}$	3.17	0.217	$\frac{5}{2}$	3.37	0.001
$\frac{5}{2}$	3.54		$\frac{5}{2}$	3.54	0.186	$\frac{3}{2}$	3.59	0.14
-	3.87		$\frac{5}{2}$	3.92	0.003	$\frac{1}{2}$	4.03	0.05
$\frac{5}{2}$	4.29		$\frac{5}{2}$	4.46	0.073	$\frac{5}{2}$	4.34	0.08
$\frac{3}{2}$	4.47		$\frac{3}{2}$	4.89	0.001	$\frac{3}{2}$	4.64	0.12

$3/2^+$ level mentioned above or the $5/2^+$ member of the $\alpha = 9$ band.

Parameters have been varied to study the sensitivity of the spectroscopic factors of the 0.338 and 2.41 MeV states as well as the excitations corresponding to the 0.338 and 1.73 MeV states. (S for the ground state is always very small and for the 1.73 MeV state is always zero.)

(a) The moment of inertia parameter $\frac{\hbar^2}{2\mathcal{I}}$ for the ground state band was varied from 0.19 to 0.23 MeV while those for the other 3 bands were varied from 0.15 to 0.27 MeV. The resultant spectroscopic factor for the 0.338 MeV state changed less than 10%; that of the 2.41 MeV state does not change. There were significant changes in the excitations corresponding to the 0.338 and 1.73 MeV states.

(b) The bandhead energies were replaced by the Nilsson values. This had negligible effect on the spectroscopic factors and a small effect on the two theoretical excitations.

(c) The off-diagonal elements of the Hamiltonian matrix were varied to account for the possibility that the factor 1/2 $\left(\frac{\hbar^2}{2\mathcal{I}} + \frac{\hbar^2}{2\mathcal{I}'}\right)$ is not correct. Large variations of A_{79} and A_{76}, even down to zero, made very little difference in the spectroscopic factors, but again the two theoretical excitations were greatly affected. Variations of 10% in A_{75} yielded changes of 5% in S for the 0.338 MeV level. It should be noted that it is mainly the mixing between the $\alpha = 5$ band and the $\alpha = 7$ band that helps to depress the first $5/2^+$ state towards its experimental value.

(d) The values of U_α^2 were varied since these are only estimates. A change of $\pm$ 0.1 for all 4 bands simultaneously yielded variations in S of 30% and 10% for the 0.338 and 2.41 MeV states respectively. This is by far the largest source of uncertainty for the spectroscopic factors, although not changing excitations significantly. The heaviest dependence lies in the choice of U_α^2 for the ground state band. All one can say is that the values of U_α^2 originally chosen are felt to be reasonable.

Besides the above points, another source of uncertainty in the theoretical spectroscopic factors is the $\langle\phi_B|\phi_A\rangle$ vibrational overlap factor, which could take on a value less than unity if there is an appreciable deformation change between the ^{20}Ne core and the ^{21}Na states. This would most probably happen for the higher excited states if at all.

CHAPTER VI

THE SHELL MODEL

A Shell Model calculation including configuration mixing was done by S.S.M. Wong (Bu 68) using a program written by French *et al* (Fr 68). Spectroscopic factors and energy level excitations were obtained and are shown in table 5-3. A comparison between the predictions of this model and experimental results shows that this model has very good success for ^{21}Na. It is noteworthy that in this calculation, a realistic effective interaction has been used and there are no adjustable parameters. Table 6-1 shows the sums of the strengths for the addition of one nucleon, $\sum S_i$, and the centroids of the one-nucleon transfer strengths $\overline{E}$ for the 3 orbits of interest, where

$$\sum_i S_i{}^j = \frac{n_h{}^j}{2j + 1} \qquad (6.1\text{-}1)$$

and

$$\overline{E} = \frac{\sum_i S_i E_i}{\sum_i S_i} \qquad (6.1\text{-}2)$$

where $n_h{}^j$ is the number of holes in the j^{th} orbit and E_i is the excitation energy of the i^{th} final state.

TABLE 6-1

Shell Model Predictions

Orbit	$\sum S_i$	$\overline{E}$(MeV)
$1d_{\frac{3}{2}}$	0.45	6.79
$1d_{\frac{5}{2}}$	0.40	1.53
$2s_{\frac{1}{2}}$	0.39	2.87

CHAPTER VII

SUMMARY AND CONCLUSIONS

There is good agreement between the experimental results, the predictions of the HF and DWBA theories and predictions of the Nilsson and Shell models of the nucleus. The Nilsson and Shell Model spectroscopic factor predictions are close to those extracted using experimental data plus a combination of DWBA and HF theories. Low-lying energy level excitations of ^{21}Na are predicted fairly well by both the Nilsson and Shell Models.

Howard *et al* (Ho 65) has shown that in the case of gamma-and beta-transitions, the Nilsson model agrees closely with experiment for ^{21}Na, ^{21}Ne and ^{23}Na. Thus the overall success of this model for odd mass nuclei with A = 21, 23 is good.

The agreement between the Shell Model predictions and experimental results gives us confidence in the Shell Model. The fact that there have been no parameter variations means that we have a particularly stringent test of the Model.

The spectroscopic factor agreement depends upon how good the DWBA and HF theories are. The predicted DWBA angular distributions fit the experimental data well for the 0.338 and 2.41 MeV states of ^{21}Na, while the HF calculation for these two states shows that the compound nucleus contribution is very small. This gives us confidence in the DWBA calculation. The case of the 1.73 MeV state is especially interesting since

it is predicted to have S = 0 by both structure models and is therefore a good test of the HF theory. The HF calculation comes close to the experimental points, thus giving us confidence in the theory. The HF calculation is also of about the right magnitude for the ground state. The shapes of the experimental angular distributions for this state and their changing with E_d indicate possible interference effects coming into play. Nilsson and Shell Model spectroscopic factor predictions of 0.003 and 0.009 are consistent with this.

Regarding parameter sets, those used in the HF, DWBA and Nilsson Model calculations are felt to be reasonable. In addition, it is shown that the sensitivity of the calculated spectroscopic factors to reasonable changes in the parameters, except for $U_\alpha{}^2$ in the Nilsson Model, is quite small. The agreement between the Nilsson and Shell Models for the low-lying levels indicates that our $U_\alpha{}^2$ are well-chosen since the two calculations are quite similar.

With respect to the higher excited states of ^{21}Na (i.e. those states less than 5 MeV excitation not studied experimentally here), the spectroscopic factor predictions of the Nilsson and Shell Models are not in very good agreement with each other. The Shell Model predicts that most of the strengths of the $1d_{\frac{5}{2}}$ and $2s_{\frac{1}{2}}$ transfers are concentrated in the 0.338 and 2.41 MeV states respectively. For the $1d_{\frac{3}{2}}$ transfer, the centroid lies at a high excitation (table 5-4) meaning that any angular distributions above E_x = 3 MeV indicating an ℓ = 2 transfer would correspond to a spin assignment of $3/2^+$. The Nilsson Model, on the other hand, predicts a rather strong I = 5/2 transfer at 3.5 MeV

besides the one at low excitation. Further experimental evidence is necessary in this respect, although it is not clear yet whether reliable spectroscopic factors can be extracted from experiments for unbound states. Level excitations for the higher states seem to agree with the model predictions for the most part. The Nilsson Model predicts a $3/2^+$ state near 3.2 MeV for which there is no corresponding state found experimentally. The Shell Model predicts a $1/2^+$ level at 4.03 MeV; the only $1/2^+$ experimental state above the 2.41 MeV state and below 5 MeV lies at 2.81 MeV. Thus it is difficult to choose correspondences between these higher states and the model-predicted higher states at present.

Finally, no conclusion can be drawn about the existence of a doublet at 2.41 MeV. Resolution must be improved before this can be determined. Pronko *et al* (Pr 67) have assigned a spin of 3/2 to the second member of the analog doublet in ^{21}Ne, but the models do not predict a positive parity state of this nature at this excitation.

APPENDIX I

DWBA THEORY

DWBA theory assumes that:

(1) elastic scattering predominates - the initial state wave function is equal to the elastic scattering wave function.

(2) the relative motion of the nuclei before and after the event is described by distorted waves, which are calculated in an optical model approximation (the effect of the target nucleons is approximated by a two-body potential).

Following Satchler (Sa 64), the DWBA theory of the reaction A(a,b)B is based on the transition amplitude of the form

$$T = J\int d\vec{r}_a \int d\vec{r}_b \; \chi_b^*(\vec{k}_b,\vec{r}_b)\langle B,b|V|A,a\rangle\chi_a(\vec{k}_a,\vec{r}_a) \qquad (A.1\text{-}1)$$

where $\vec{r}_a$ is the displacement of 'a' from 'A', $\vec{r}_b$ is the displacement of 'b' from 'B' and J is the Jacobian of the transformation to these relative coordinates. $\chi_{a,b}$ are the distorted waves which, in the optical model approximation, are generated from the Schroedinger equation:

$$\{\nabla^2 + k^2 - \frac{2\mu}{\hbar^2}[U(r) + U_c(r)]\}\,\chi(\vec{k},\vec{r}) = 0 \qquad (A.1\text{-}2)$$

where $U(r)$ is the optical potential, $U_c(r)$ the Coulomb potential and μ the reduced mass of the pair.

The remaining factor in (A.1-1) is the matrix element of the interaction causing the inelastic event, taken between the internal states of the colliding pairs:

$$\langle B,b|V|A,a\rangle = \int \psi_B^* \psi_b^* V \psi_A \psi_a d\xi \qquad \text{(A.1-3)}$$

where ξ respresents all the coordinates independent of $\vec{r}_a$ and $\vec{r}_b$. This factor, a function of $\vec{r}_a$ and $\vec{r}_b$, plays the role of an effective interaction for the transition between the elastic scattering states χ_a and χ_b. The 'Physics' of the reaction appears in the magnitude and radial shape of this factor.

The differential cross-section for unpolarized projectiles and target nuclei is:

$$\frac{d\sigma}{d\Omega} = \frac{\mu_a \mu_b}{(2\pi\hbar^2)^2} \cdot \frac{k_b}{k_a} \cdot \frac{\sum |T|^2}{(2J_A+1)(2s_a+1)} \qquad \text{(A.1-4)}$$

where J_A and s_a are the spins of 'A' and 'a' and the sum is over the z-components of the spins of A, a, B, b. This can also be written (Sa 64):

$$\frac{d\sigma}{d\Omega} = \frac{\mu_a \mu_b}{(2\pi\hbar^2)^2} \cdot \frac{k_b}{k_a} \cdot \frac{2J_B+1}{2J_A+1} \sum_j \frac{|A_{\ell sj}|^2}{2s_a+1} \sum_{m m_b m_a} |\beta_{sj}^{\ell m m_b m_a}|^2 \qquad \text{(A.1-5)}$$

where $\vec{j} = \vec{J}_B - \vec{J}_A$, $\vec{s} = \vec{s}_a - \vec{s}_b$, $\vec{\ell} = \vec{j} - \vec{s}$, $m = M_B - M_A + m_b - m_a$, the M, m's are z-components of spins, the $A_{\ell sj}$ are related to the spectroscopic factors $S_{\ell j}$ and the $\beta_{sj}^{\ell m m_b m_a}$ contain the integrals of the elastic scattering wave functions and the radial form factors for V.

To compute the cross-sections, we use a partial wave expansion for the distorted waves χ, where the partial waves are solutions of the Schroedinger equation with the constraints that they are zero at r = 0 and for large r, the partial waves are:

$$\chi_{LJ}(k,r) = \frac{i}{2}\left[H_L^*(kr) + \eta_L^J H_L(kr)\right] \exp(i\sigma_L) \qquad (A.1\text{-}6)$$

where $H_L = G_L + iF_L$ is the outgoing wave Coulomb function, σ_L is the Coulomb phase shift and η_L^J is the reflection coefficient or scattering matrix element for the (L,J) wave. The η_L^J are computed by numerically integrating the Schroedinger equation and matching the function and its derivative to the form (A.1-6) at large r.

We have been considering the general case A(a,b)B. Let us now consider the special case of the A(d,n)B stripping reaction. A commonly used method of deriving an approximate amplitude of T gives the final state interaction potential $V = V_{nB} - U_{nB}$ where U_{nB} is the optical potential used to generate χ_n. Then

$$V = V_{pn} + V_{nA} - U_{nB} \simeq V_{pn} \qquad (A.1\text{-}7)$$

since V_{pn} dominates (there is considerable cancellation between V_{nA} and U_{nB}). We can now write, following (A.1-3),

$$J\langle B,n|V|A,d\rangle = J\int d\xi_A \psi^{B*}_{J_B M_B}(\vec{r}_{pA},\sigma_p,\xi_A)\psi^{n*}_{\frac{1}{2}\, m_{\frac{1}{2}}}(\sigma_n)V(r_{np})\psi^{A}_{J_A M_A}(\xi_A)$$

$$\cdot\, \psi^{d}_{lm_l}(\vec{r}_{np},\sigma_p,\sigma_n) \qquad (A.1\text{-}8)$$

where ξ_A represents the internal coordinates of A, $\sigma_{p,n}$ represents the spin structure of the proton (neutron), J corresponds to the transformation from $\vec{r}_{pA}$, $\vec{r}_{np}$ to $\vec{r}_n$, $\vec{r}_d$ and is given by:

$$J = \left(\frac{M_d M_A}{M_p(M_d+M_A)}\right)^3 \qquad \text{(A.1-9)}$$

where the M's are masses.

By expanding ψ^B in terms of the eigenstates of ψ^A and the wave function of the captured proton and expanding the latter into spherical harmonics in $\vec{r}_{pA}$, it can be shown (Sa 64) that

$$J\langle B,n|V|A,d\rangle \sim n^{\frac{1}{2}}\alpha_{\ell j}\, u_{\ell j}(r_{pA})Y_\ell^{m*}(\vec{r}_{np})V(r_{np})\,\phi_d(r_{np}) \qquad \text{(A.1-10)}$$

where 'n' is the number of equivalent nucleons in orbit (ℓ,j), $u_{\ell j}$ is the radial function of the shell model orbit, $\alpha_{\ell j}$ is a fractional parentage coefficient and

$$\phi_d(r_{np}) = N\left\{\frac{e^{-\alpha r_{np}}-e^{-\beta r_{np}}}{r_{np}}\right\} \qquad \text{(A.1-11)}$$

is the Hulthén wave function, where

$$N = \left[\frac{\alpha\beta(\alpha+\beta)}{\pi(\beta-\alpha)}\right]^{\frac{1}{2}} \qquad \text{(A.1-12)}$$

where $\alpha = \sqrt{\frac{M\varepsilon_d}{\hbar^2}}$, M = nucleon mass, ε_d = deuteron binding energy and $\beta = 7\alpha$. ($\psi^d = \phi_d(r_{np})\phi_{lm_l}$ if only the deuteron S-state is considered.)

The usual spectroscopic factor is:

$$S_{\ell j} = n(\alpha_{\ell j})^2 \qquad \text{(A.1-13)}$$

In the zero-range approximation,

$$V(r_{np})\phi_d(r_{np}) = D_0\ \delta(r_{np}) \qquad \text{(A.1-14)}$$

where $D_0{}^2 = \left(1 + \frac{\alpha}{\beta}\right)^3 \left(\frac{\hbar^2}{M}\right) 8\pi\alpha = 1.53 \times 10^4\ \text{MeV}^2\text{-fm}^3$.

The 'finite range' approximation (Bu 64) differs only in the multiplicative factor which is applied to the radial form factor:

$$\Lambda(r) = 1 - \left[\frac{U_d(r) - U_n\left(\frac{M_A}{M_B}\, r\right) - U_p(r) - \varepsilon_d}{(\beta^2/\alpha^2)\varepsilon_d}\right] \qquad \text{(A.1-15)}$$

where $U_i(r)$ are optical model potentials.

The local optical model potentials introduced have been found to have strengths which vary with bombarding energy. This is partly because the potential is non-local and partly because of an intrinsic energy dependence. In the non-local approximation, we use local optical potentials but take into account the damping of the wave functions in the nuclear interior which would arise from using equivalent non-local potentials (Pe 62). The damping factor has the form (Hj 65):

$$f(r) = C\left(1 - \frac{1}{2}\, U(r)\, \frac{m\beta^2}{\hbar^2}\right)^{\frac{1}{2}} \qquad \text{(A.1-16)}$$

for each of the three wave functions appearing in the stripping amplitude. $U(r)$ is the corresponding local potential and β is the range of the nonlocality. C is unity for scattering wave functions but is adjusted

to preserve the normalization for the bound state wave function. Usual values of β are 0.85 fm. for the neutron and proton and 0.54 fm. for the deuteron.

The optical model potential most often used has a potential well radial dependence of Woods-Saxon type. Its form is:

$$U(r) = \frac{V}{e^{x}+1} + iW_D \frac{d}{dx'}\left(\frac{1}{e^{x'}+1}\right) + \frac{iW}{e^{x'}+1} - (V_s+iW_s)\frac{1}{r}\frac{d}{dr}\left(\frac{1}{e^{x}+1}\right) \cdot \vec{L}\cdot\vec{S} \qquad \text{(A.1-17)}$$

where $x = \frac{r-r_0 A^{\frac{1}{3}}}{a}$, a = 'diffuseness' of the well.

The first term corresponds to volume potential scattering, the second to surface absorption, the third to volume absorption and the last to spin-orbit scattering. For low bombarding energies, there is expected to be no volume absorption. The parameters V, W_D, V_s, W_s, r_0, r_0', a, a' for the incoming and outgoing channels are taken from elastic scattering work at the appropriate energy, but in practice should be averages over an energy range.

The Coulomb potential is taken to be that arising from a uniformly charged sphere of radius $R_c = r_c A^{\frac{1}{3}}$. For the incoming channel, for instance,

$$U_c(r) = \begin{cases} \frac{Z_d Z_A e^2}{2R_c}\left\{3 - \frac{r^2}{R_c^2}\right\} & \text{for } r<R_c \\ \frac{Z_d Z_A e^2}{R_c} & \text{for } r>R_c \end{cases} \qquad \text{(A.1-18)}$$

APPENDIX II

HAUSER-FESHBACH THEORY

In a direct reaction, a projectile interacts with one or a few of the surface nucleonsas it passes the target nucleus, the entire process taking about 10^{-22} sec. On the other hand, in a compound nucleus reaction, the projectile 'dissolves' into the target nucleus, many interactions take place, and at some later time (about 10^{-19} sec.) a particle may be emitted. By the time this happens, the mode of formation likely has been forgotten but spin and parity are still conserved. The intermediate nucleus formed by the target nucleus and projectile is called the 'compound nucleus'.

Let $\vec{J},\pi$ be the spin and parity of the compound nucleus and $\vec{J}_\alpha$ and $\vec{S}_\alpha$ be the spins of the target nucleus and projectile in channel α. For an orbital angular momentum $\vec{\ell}_\alpha$, we have

$$\vec{\ell}_\alpha + \vec{S}_\alpha = \vec{j}_\alpha \; ; \quad \vec{j}_\alpha + \vec{J}_\alpha = \vec{J} \qquad \text{(A.2-1)}$$

Assume that, at the excitation energy of the compound nucleus, there are many energy levels of all types. In other words, the energy resolution of the incident beam is broad enough so that many levels of the compound nucleus are excited. The corresponding wave functions are assumed to have random phase so that when phase averages are performed all interference terms will vanish. Hence, the ℓ_α will not interfere in

the formation or decay of the compound nucleus (Ha 52).

Let $\alpha = 1$ be the bombarding channel, $\alpha = 2$ the observed channel, k the wave number and $T_{\ell_\alpha j_\alpha}$ the penetrability for partial wave ℓ_α and total spin j_α. Then the differential cross-section for emission in the solid angle $d\Omega$ can be written (Sm 65a):

$$\frac{d\sigma(\theta)}{d\Omega} = \frac{1}{4k^2(2J_1+1)(2S_1+1)} \sum_\nu A_\nu P_\nu(\cos\theta) \qquad \text{(A.2-2)}$$

where P_ν are Legendre polynomials and

$$A_\nu = \sum_{J,\pi} \frac{2J+1}{D_{J\pi}} \cdot D_1 \cdot D_2 \qquad \text{(A.2-3)}$$

where $D_1 = \sum_{\ell_1 j_1} \beta_\nu{}^{J_1 S_1}(\ell_1 j_1 J) T_{\ell_1 j_1}$; $D_2 = \sum_{\ell_2 j_2} \beta_\nu{}^{J_2 S_2}(\ell_2 j_2 J) T_{\ell_2 j_2}$ (A.2-4)

$\beta_\nu{}^{J\alpha S\alpha}(\ell_\alpha j_\alpha J)$ are angular momentum coupling coefficients and

$$D_{J\pi} = \sum_{\alpha,\ell_\alpha,j_\alpha} T_{\ell_\alpha j_\alpha} \qquad \text{(A.2-5)}$$

is the sum over all penetrabilities with subscripts which can be coupled to form a compound state with spin and parity J,π in the manner of (A.2-1)

From the compound nucleus concept, the reaction process has been divided into two parts - the formation and the decay of the compound nucleus. For a compound nucleus level of spin J, $\frac{D_2}{D_{J\pi}}$ in (A.2-2)

represents the probability that channel $\alpha = 2$ is selected out of all the possible outgoing channels and $\frac{(2J+1)}{k^2(2J_1+1)(2S_1+1)} \cdot D_1$ represents the probability of formation of the compound nucleus.

A consequence of the statistical assumption is that the angular distribution is symmetrical about 90°. i.e. ν = even in (A.2-2) (Pr 62a). That the distribution is peaked at 0° can be seen (Er 60) by assuming the reaction proceeds through only one level of the compound nucleus and that the initial spins J_1 and S_1 are zero. $\vec{J}$ will be equal to $\vec{\ell}_1$ and will therefore be perpendicular to the beam direction. If J_2 and S_2 are zero and the outgoing particle moves in a direction $\vec{n}$, the differential cross-section will be proportional to $\int \delta(\vec{n}\cdot\vec{J})d\phi$ where δ is the Dirac Delta-function, ϕ is the azimuthal angle about the beam direction. This results in $\frac{d\sigma}{d\Omega} \sim \frac{1}{\sin\theta}$ where θ is the angle between $\vec{n}$ and the beam direction. Thus the distribution is symmetrical about 90° for this special case and sharply peaked at 0° and 180° (except where $\ell_1 = 0$ in which case its isotropic). With non-zero J_α and S_α, the distribution will be smeared out but still symmetrical about 90°. All compound nucleus levels of spin $\vec{J}$ will contribute symmetrical distributions. However, where there is appreciable interference between their corresponding waves, the distribution need not be symmetrical about 90°. In the HF calculation, this type of interference cancels out on the average. For a general discussion on angular distributions, see (Er 60).

Where spin-parities and excitations of the residual nuclei are not known, we must incorporate level density expressions into (A.2-5). It is found (Da 68) that to a good approximation to the expression given by

Newton (Ne 56), especially at higher excitation energies:

$$\ell n_{10}\, N(E_x) = a + b\sqrt{E_x} \qquad \text{(A.2-6)}$$

where $N(E_x)$ is the number of levels below E_x. Thus the level density as a function of excitation energy is:

$$\rho(E_x) = \frac{dN(E_x)}{dE_x} = \frac{1.15b}{\sqrt{E_x}} \exp[2.30(a+b\sqrt{E_x})] \qquad \text{(A.2-7)}$$

The distribution of spins is taken, for a nucleus in channel α, to be:

$$\rho(E_x,J_\alpha) = (2J_\alpha+1)\exp\left[-\frac{J_\alpha(J_\alpha+1)}{2\sigma^2}\right]\rho(E_x) \qquad \text{(A.2-8)}$$

where σ, called the 'spin-cutoff parameter', is proportional to $E_x^{\frac{1}{4}}$. $\sigma \approx 2.5$ for $E_x = 10$ MeV (Da 68). Finally, expression (A.2-5) becomes

$$D_{J\pi} = \int_{E_{beg.}}^{E_{end}} \sum_{\alpha,j_\alpha,\ell_\alpha} T_{\ell_\alpha,j_\alpha}\, \rho(E_x,J_\alpha)\,dE_x \qquad \text{(A.2-9)}$$

where $E_{end} = E_a + Q_{A,a \to B,b}$ and $E_{beg.}$ is the energy above which spin-parities and excitations are not known.

Let us now determine how we get the penetrabilities. The solution $\chi_{\ell j}$ of the scattering radial Schroedinger equation has the two boundary conditions (Sm 65a):

(1) $\chi_{\ell j}(0) = 0$

(2) $\chi_{\ell j}(r)$ is proportional for large r, to $a(F_\ell+iG_\ell) + b(F_\ell-iG_\ell)$

where F_ℓ, G_ℓ are the regular and irregular Coulomb wave functions and

a,b are boundary matching constants. $F_\ell+iG_\ell$ represents an incoming wave and $F_\ell-iG_\ell$, an outgoing 'reflected' wave. The expression in (2) can be written

$$F_\ell - \beta_{\ell j}(F_\ell - iG_\ell) \quad \text{where} \quad a = \frac{1}{2} \quad \text{and} \quad b = \frac{1}{2}(1-2\beta_{\ell j}).$$

The corresponding penetrability is

$$T_{\ell j} = 1 - \left|\frac{b}{a}\right|^2 = 1 - \left|1-2(\mathrm{Re}\beta_{\ell j} + i\ \mathrm{Im}\beta_{\ell j})\right|^2$$

$$= 4[\mathrm{Re}\beta_{\ell j} - ((\mathrm{Re}\beta_{\ell j})^2 + (\mathrm{Im}\beta_{\ell j})^2)] \qquad \text{(A.2-10)}$$

$\beta_{\ell j}$ is determined by solving (Sm 65a):

$$\frac{\chi_{\ell j}(r_1)}{\chi_{\ell j}(r_2)} = \frac{F_\ell(r_1) - \beta_{\ell j}[F_\ell(r_1) - iG_\ell(r_1)]}{F_\ell(r_2) - \beta_{\ell j}[F_\ell(r_2) - iG_\ell(r_2)]} \qquad \text{(A.2.11)}$$

APPENDIX III

NILSSON MODEL THEORY

In the Nilsson Model, the collective rotational energy of the 'core' and the single particle energies due to extra-core nucleons are separated. The wave equation for the nucleus is (Pr 62):

$$(T_{ROT} + \sum_{p} H_p)\psi = E\psi \qquad \text{(A.3-1)}$$

where

$$T_{ROT} = \sum_{k=1}^{3} \frac{R_k^2}{2\mathcal{J}_k} = \sum_{k=1}^{3} \frac{(J_k - j_k)^2}{2\mathcal{J}_k} \quad , \qquad \text{(A.3-2)}$$

$\vec{J}$, $\vec{R}$ and $\vec{j}$ are the total, core and particle angular momenta and $\mathcal{J}$ is the moment of inertia. In the case of axial symmetry and with the usual notation, $j_3 = \Omega$ and $J_3 = K$ we have:

$$T_{ROT} = \frac{\hbar^2}{2\mathcal{J}}[J(J+1) - K^2 - \Omega^2] + \frac{\hbar^2}{2\mathcal{J}_3}(K - \Omega)^2 - \frac{\hbar^2}{2\mathcal{J}}(J_+j_- + J_-j_+) + \frac{\hbar^2}{2\mathcal{J}}\vec{j}^{\,2} \qquad \text{(A.3-3)}$$

where Ω, K and J^2 are constants of motion, $J_{\pm}$ ($= J_1 \pm iJ_2$) and $j_{\pm}$ ($= j_1 \pm ij_2$) are operators. The term involving these operators couples rotational and particle angular momenta and is called the RPC term - to first order, it couples states of a given J with a difference in K of 1 or with $K = K' = 1/2$. The term in $\vec{j}^{\,2}$ contains only particle

coordinates and can be absorbed in the particle Hamiltonian. We have:

$$\left(\frac{\hbar^2}{2\mathcal{J}}\left[J(J+1) - K^2-\Omega^2\right] + \frac{\hbar^2}{2\mathcal{J}_3}\left[K-\Omega\right]^2 + H_0+RPC\right)\psi = E\psi \qquad (A.3\text{-}4)$$

where $$H_0 = \sum_p H_p + \frac{\hbar^2}{2\mathcal{J}}\left(\sum_p \vec{j}_p\right)^2 \qquad (A.3\text{-}5)$$

For low-lying states $\mathcal{J}_3$ is small, thus $K = \Omega$ i.e. there is no component of collective angular momentum along the symmetry axis.

The normalized intrinsic wave function is defined by

$$H_0\left|K\pi\alpha\right> = E_0\left|K\pi\alpha\right> \qquad (A.3\text{-}6)$$

where the $K\pi\alpha$ refer to a specific Nilsson Model orbital. (K,π are the spin and parity; α is the orbital number). Each single particle function $\left|K\pi\alpha\right>$ can be expanded in terms of the spherical limit Shell Model functions:

$$\left|K\pi\alpha\right> = \sum_{N\ell j} \left<N\ell j\middle|K\pi\alpha\right>\left|N\ell j\right> \qquad (A.3\text{-}7)$$

where N, ℓ, j are the usual Shell Model quantum numbers. In the Nilsson Model representation (Ni 55):

$$\left|K\pi\alpha\right> = \sum_{\ell\Lambda} a_{\ell\Lambda}\left|N\ell\Lambda\Sigma\right> \qquad (A.3\text{-}8)$$

where $\sum_{\ell\Lambda} a^2_{\ell\Lambda} = 1$ and the constants of motion are ℓ, $\Lambda(=\ell_3)$ and $\Sigma(=s_3)$. The $\left<N\ell j\middle|K\pi\alpha\right>$ coefficients are connected to the normalized Nilsson coefficients $a_{\ell\Lambda}$ by angular momentum addition relations:

$$\left<N\ell j\middle|K\pi\alpha\right> = \sum_{\ell\Lambda} \left(\ell\tfrac{1}{2}\Lambda\Sigma\middle|jK\right)a_{\ell\Lambda} \qquad (A.3\text{-}9)$$

The energy eigenvalues for the axially symmetric nucleus in the absence of RPC between different states are:

$$E(NJK\alpha) = E_0(NK\alpha) + \frac{\hbar^2}{2\mathcal{J}} [J(J+1) - 2K^2 + \delta_{K,\frac{1}{2}} a(-1)^{J+\frac{1}{2}}(J+\tfrac{1}{2})] \qquad (A.3\text{-}10)$$

where the 'decoupling parameter',

$$a = -\sum_j (-1)^{j+\frac{1}{2}} (j+\tfrac{1}{2}) \langle N\ell j | K\pi\alpha\rangle^2 \qquad (A.3\text{-}11)$$

is the contribution of the RPC term when $K = \frac{1}{2}$. Equation (A.3-10) shows that a rotational band with $J = K, K+1, \ldots$ is built upon each particle state of spin K.

Nilsson (Ni 55) lists the coefficients $a_{\ell\Lambda}$, in unnormalized form, and the numbers $r(NK\alpha)$ as a function of the core deformation η and the strength of the ℓ^2-splitting term μ, where the Nilsson eigenvalues are given by:

$$E_0(NK\alpha) = \frac{3}{4} [(N+\tfrac{3}{2})\hbar\omega_0(\delta) + \kappa\hbar\overset{0}{\omega}_0 r(NK\alpha)] \qquad (A.3\text{-}12)$$

where $\hbar\overset{0}{\omega}_0 = 41A^{-\frac{1}{3}}$ MeV, $\hbar\omega_0(\delta) = \dfrac{\hbar\overset{0}{\omega}_0 \eta\kappa}{\delta}$, κ is the strength of the $\vec{\ell}\cdot\vec{s}$ term and δ is another distortion parameter.

Let us now consider the stripping reaction A(a,b)B. By evaluating the overlap integral between the target and residual nucleus wave functions, Satchler (Sa 58) shows that for an even-even target nucleus of spin zero, the expression for the spectroscopic factor is (neglecting RPC):

$$\sqrt{S_{\ell j}} = \frac{2}{2j+1} \langle N\ell j | K\pi\alpha\rangle \, \delta(jJ) \, \langle \phi_B | \phi_A \rangle \qquad (A.3\text{-}13)$$

where $K = K_B$, $J = J_B$ and $\langle\phi_B|\phi_A\rangle$ is the overlap of the initial and final vibrational states and is usually taken to be unity for transitions to low-lying levels. We must have $j = J$ to conserve total angular momentum.

If we now introduce RPC, we must diagonalize the Hamiltonian matrix where the diagonal elements are the energies (A.3-10) and the off-diagonal elements are:

$$A^J_{\alpha'\alpha} = \langle JMK'\alpha'| \frac{\hbar^2}{2\mathcal{I}_{av.}} (J_+j_- + J_-j_+) |JMK\alpha\rangle$$

$$= -\frac{\hbar^2}{2\mathcal{I}_{av.}} \sqrt{(J+K_>)(J-K_>+1)} \left[1 - \delta_{K'K} + (-1)^{J-\frac{1}{2}} \delta_{K\frac{1}{2}}\delta_{K'\frac{1}{2}}\right] \cdot A_{\alpha'\alpha} \qquad \text{(A.3-14)}$$

where $K_>$ is the greater of K' and K, $\frac{\hbar^2}{2\mathcal{I}_{av.}}$ is taken to be $\frac{1}{2}\left(\frac{\hbar^2}{2\mathcal{I}} + \frac{\hbar^2}{2\mathcal{I}'}\right)$ (Lu 67) and

$$A_{\alpha'\alpha} = \sum_j \langle N\ell j|K'\pi\alpha'\rangle\langle N\ell j|K\pi\alpha\rangle\sqrt{(j+K)(j-K+1)}$$

$$\times \left[1 - \delta_{K'K} + (-1)^{j-\frac{1}{2}} \delta_{K\frac{1}{2}}\, \delta_{K'\frac{1}{2}}\right] \qquad \text{(A.3-15)}$$

Upon diagonalization, we get the wave functions

$$|JM\rangle = \sum_{K\alpha} C_{K\alpha} |JMK\alpha\rangle \qquad \text{(A.3-16)}$$

and the energy eigenvalues for each mixed state with spin J. With bandmixing expression (A.3-13) becomes:

$$\sqrt{S_{\ell j}} = \frac{2}{2j+1} \sum_{K\alpha} C_{K\alpha} \langle N\ell j | K\pi\alpha \rangle \delta(jJ) \qquad \text{(A.3-17)}$$

The effects of pairing are included by writing (Lu 67):

$$\sqrt{S_{\ell j}} = \frac{2}{2j+1} \sum_{K\alpha} C_{K\alpha} U_\alpha \langle N\ell j | K\pi\alpha \rangle \delta(jJ) \qquad \text{(A.3-18)}$$

where U_α^2 is the probability that a particular state is empty. The $A^J_{\alpha',\alpha}$ are modified by the multiplicative factor $(U_{\alpha'}U_\alpha + V_{\alpha'}V_\alpha)$ where $U_\alpha^2 + V_\alpha^2 = 1$.

REFERENCES

Aj 61 F. Ajzenberg-Selove, L. Cranberg and F.S. Dietrich; Phys. Rev. 124 (1961) 1548.

Be 61 R.E. Benenson and L.J. Lidofsky; Phys. Rev. 123 (1961) 939.

Bh 62 K.H. Bhatt; Nucl. Phys. 39 (1962) 375.

Br 60 J.E. Brolley and J.L. Fowler; 'Fast Neutron Physics: VI' (1960) 73.

Br 62 D.W. Braben; Nucl. Phys. 32 (1962) 584.

Bu 64 P.J.A. Buttle and L.J.B. Goldfarb; Proc. Phys. Soc. (London) A83 (1964) 701.

Bu 67 M.B. Burbank; Thesis, University of Alberta (unpublished) (1967).

Bu 68 M.B. Burbank, G.G. Frank, N.E. Davison, G.C. Neilson, S.S.M. Wong and W.J. McDonald; Nucl. Phys. (to be published).

Cl 62 A.B. Clegg and K.J. Foley; Phil. Mag. 7 (1962) 247.

Da 68 N.E. Davison; University of Ablerta Internal Report (1968).

En 62 P.M. Endt and C. Van der Leun; Nucl. Phys. 34 (1962) 1.

En 67 P.M. Endt and C. Van der Leun; Nucl. Phys. A105 (1967) 1.

Er 60 T. Ericson; Phil. Mag. Suppl. 9 (1960) 425.

Ev 55 R.D. Evans; 'The Atomic Nucleus' (1955) 661.

Fr 60 J.M. Freeman; 'Proc. of the International Conf. on Nuclear Structure' (U. of Toronto Press) (1960) 477.

Fr 68 J.B. French, E.C. Halbert, J.B. McGrory and S.S.M. Wong; (to be published).

Ge 67 D.A. Gedcke and W.J. McDonald; University of Alberta Internal Report (1967).

Ge 67a D.A. Gedcke and W.J. McDonald; Nucl. Inst. and Meth. 56 (1967) 148.

Gi 65 W.R. Gibbs and W. Grüebler; Nucl. Phys. 62 (1965) 548.

Gl 64 W. Glöckle; Z. Phys. 178 (1964) 53.

Go 60 H.E. Gove; 'Proc. of the International Conf. on Nuclear Structure' (U. of Toronto Press) (1960) 438.

Go 61 M.D. Goldburg, J.D. Anderson, J.P. Stoering and C. Wong; Phys. Rev. 122 (1961) 1510.

Gr 61 W. Grüebler and J. Rossel; Helv. Phys. Acta 34 (1961) 718.

Gr 67 T.B. Grandy and J.W.D. Sinclair; University of Alberta Internal Report (1967).

Ha 52 W. Hauser and H. Feshbach; Phys. Rev. 87 (1952) 366.

Ha 64 O. Hansen; Nucl. Phys. 51 (1964) 307.

Ha 67 E.C. Halbert; Bull. Am. Phys. Soc. 12 (1967) 1192.

Hj 65 S.A. Hjorth, J.X. Saladin and G.R. Satchler; Phys. Rev. 138 (1965) B1425.

Ho 65 A.J. Howard, J.P. Allen and D.A. Bromley; Phys. Rev. 139 (1965) B1135.

Ho 65a A.J. Howard, D.A. Bromley and E.K. Warburton; Phys. Rev. 137 (1965) B32.

Ho 67 A.J. Howard, J.P. Allen, D.A. Bromley, J.W. Olness and E.K. Warburton; Phys. Rev. 157 (1967) 1022.

Ke 64 I. Kelson and C.A. Levinson; Phys. Rev. 134 (1964) B269.

Ku 67 T.T.S. Kuo; Nucl. Phys. A103 (1967) 71.

Ku 67a P.D. Kunz; University of Colorado, private communication.

La 65 H. Lancman; Nucl. Phys. 69 (1965) 384.

Li 58 A.E. Litherland, H. McManus, E.B. Paul, D.A. Bromley and H.E. Gove; Can. J. Phys. 36 (1958) 378.

Lu 67 H.F. Lutz, J.J. Wesolowski, L.F. Hanson and S.F. Eccles; Nucl. Phys. A95 (1967) 591.

Ma 66 C. Maples, G.W. Goth and J. Cerny; Lawrence Radiation Laboratory Report UCRL 16964 (July, 1966).

Mc 67 W.J. McDonald and D.A. Gedcke; Nucl. Inst. and Meth. 55 (1967) 1.

Ne 56 T.D. Newton; Can. J. Phys. 34 (1956) 804.

Ni 55 S.G. Nilsson; K.D.V.S. Mat. Fys. Medd. 29 #16 (1955).

Pa 58 E.B. Paul and J.H. Montague; Nucl. Phys. 8 (1958) 61.

Pe 62 F. Perey and B. Buck; Nucl. Phys. 32 (1962) 353.

Pe 65 E. Farrelly Pessoa; Nucl. Phys. 68 (1965) 337.

Pe 65a D. Pelte and B. Povh; Nucl. Phys. 73 (1965) 492.

Pr 62 M.A. Preston; 'Physics of the Nucleus' (1962) 255.

Pr 62a M.A. Preston; 'Physics of the Nucleus' (1962) 514.

Pr 67 J.G. Pronko, C. Rolfs and H.J. Maier; Nucl. Phys. A94 (1967) 561.

Ro 66 L. Rosen; 'Second International Symposium on Polarization Phenomena of Nucleons' (1966) 278.

Sa 58 G.R. Satchler; Ann. Phys. 3 (1958) 275.

Sa 64 G.R. Satchler; Nucl. Phys. 55 (1964) 1.

Sm 65 W.R. Smith; Oak Ridge National Laboratory Internal Report ORNL-TM-1234 (1965).

Sm 65a W.R. Smith; Oak Ridge National Laboratory Internal Report ORNL-TM-1117.

Te 66 J.W. Tepel; Nucl. Inst. and Meth. 40 (1966) 100.

Va 64 C. Van der Leun and W.L. Mouton; Physica 30 (1964) 333.

Wo 68 S.S.M. Wong; University of Alberta Internal Report (1968).

Wh 58 W. Whaling; Handbuch der Phys. 34 (1958) 193.

Ya 51 B. Yaramis; Phys. Rev. 124 (1961) 836.